

Gravitational waves \times HI intensity mapping: cosmological and astrophysical applications

Giulio Scelfo,^{a,b,c} Marta Spinelli,^{d,b,c,e} Alvise Raccanelli,^{f,g,h}
Lumen Boco,^{a,b,c} Andrea Lapi,^{a,b,c,i} Matteo Viel^{a,b,c,d}

^aSISSA, Via Bonomea 265, 34136 Trieste, Italy

^bINFN, Sezione di Trieste, Via Bonomea 265, 34136 Trieste, Italy

^cIFPU, Institute for Fundamental Physics of the Universe, via Beirut 2, 34151, Trieste, Italy

^dINAF/OATS, Osservatorio Astronomico di Trieste, via Tiepolo 11, I-34143 Trieste, Italy

^eDepartment of Physics and Astronomy, University of the Western Cape, Robert Sobukhwe Road, Bellville, 7535, South Africa

^fDipartimento di Fisica e Astronomia “Galileo Galilei”, Università degli Studi di Padova, via Marzolo 8, I-35131, Padova, Italy

^gINFN, Sezione di Padova, via F. Marzolo 8, I-35131 Padova, Italy.

^hTheoretical Physics Department, CERN, 1 Esplanade des Particules, 1211 Geneva 23, Switzerland

ⁱINAF/IRA, via Gobetti 101, 40129 Bologna, Italy

E-mail: giulio.scelfo@sissa.it, marta.spinelli@inaf.it, alvise.raccanelli.1@unipd.it,
lboco@sissa.it, lapi@sissa.it, viel@sissa.it

Abstract. Two of the most rapidly growing observables in cosmology and astrophysics are gravitational waves (GW) and the neutral hydrogen (HI) distribution. In this work, we investigate the cross-correlation between resolved gravitational wave detections and HI signal from intensity mapping (IM) experiments. By using a tomographic approach with angular power spectra, including all projection effects, we explore possible applications of the combination of the Einstein Telescope and the SKAO intensity mapping surveys. We focus on three main topics: *(i)* statistical inference of the observed redshift distribution of GWs; *(ii)* constraints on dynamical dark energy models as an example of cosmological studies; *(iii)* determination of the nature of the progenitors of merging binary black holes, distinguishing between primordial and astrophysical origin. Our results show that: *(i)* the GW redshift distribution can be calibrated with good accuracy at low redshifts, without any assumptions on cosmology or astrophysics, potentially providing a way to probe astrophysical and cosmological models; *(ii)* the constraints on the dynamical dark energy parameters are competitive with IM-only experiments, in a complementary way and potentially with less systematics; *(iii)* it will be possible to detect a relatively small abundance of primordial black holes within the gravitational waves from resolved mergers. Our results extend towards GW \times IM the promising field of multi-tracing cosmology and astrophysics, which has the major advantage of allowing scientific investigations in ways that would not be possible by looking at single observables separately.

Contents

1	Introduction	1
2	Methodology	3
2.1	Angular power spectra	3
2.2	Fisher analysis	6
3	Observables	6
3.1	Gravitational Waves	7
3.2	HI Intensity Mapping	9
3.2.1	From resolved sources to IM	10
3.2.2	Noise sources	11
4	Gravitational waves statistical redshift distribution	13
5	Cosmological constraints: dynamical dark energy	15
6	Astrophysical vs. primordial origin of merging black hole binaries	18
6.1	Progenitors	19
6.1.1	Astrophysical scenario	19
6.1.2	Primordial scenario: “early” binaries	20
6.1.3	Primordial scenario: “late” binaries	20
6.1.4	Primordial scenario: “mixed” binaries	21
6.2	Forecasts	21
7	Conclusions	22
A	Relativistic number counts	25
B	Astrophysical vs. primordial BBHs: “early” primordial scenario as fiducial	25

1 Introduction

Since the first detection of gravitational waves (GWs), originated from the merger of a Binary Black Hole (BBH) of a total mass $M_{\text{tot}} \sim 60M_{\odot}$ [1, 2] the interest towards the use of GWs in astrophysics and cosmology has surged, due to the possibility of studying the Universe through a new observational channel. Several detections have been made since then [3, 4], opening the scientific path of gravitational waves astronomy.

Another observable that has recently emerged as extremely promising is the measurement of the integrated emission from spectral lines coming from unresolved galaxies and the diffuse intergalactic medium, the so-called Intensity Mapping (IM - see e.g., [5] for a comprehensive review). The IM technique allows probing large areas of the sky in a relatively small amount of time, since it does not aim at resolving single galaxies: it measures the intensity of a specific emission line in order to map the underlying matter distribution, treating it as a diffuse background. Since we exactly know the emission frequency of the line under study, the observed wavelength provides information on the radial position of the source, whereas its

brightness temperature fluctuations describe how the underlying Large Scale Structure (LSS) is distributed. The redshifted 21 cm line of neutral hydrogen is one of the most promising targets for IM and several detections of the signal in cross-correlation with galaxy surveys have already been achieved (see e.g., [6–9]). This tool potentially allows us to trace the LSS over a vast range of redshifts, and for the focus of this work, from the end of the reionization epoch ($z \sim 6$) to the present day [10]. IM surveys have been proposed for the forthcoming Square Kilometre Array Observatory (SKAO) [11] and are ongoing on its precursor MeerKAT [12, 13], potentially bringing exquisite constraints for Cosmology [14–16]. Other purpose-built experiments are taking data or will be build in the near future e.g. CHIME [17], FAST [18], BINGO [19], Tianlai [20] and HIRAX [21].

Given the rapidly growing interest in both GW and IM, it is natural to investigate the synergies and the scientific output that can be obtained through their combination. In fact, cross-correlations of different tracers have been used already as a probe for cosmology. For example, the cross-correlation between e.g., the LSS and the Cosmic Microwave Background (see e.g., [22–31]), neutrinos (see e.g., [32]), various LSS tracers (see e.g., [33–36]) and even GWs (see e.g., [37–50]). Finally, also the IM technique has been the subject of cross-correlation studies, such as e.g., [51–63].

The advantage of considering maps of emission line intensity as observables is not limited to the fact that they provide another LSS tracer. Intensity mapping measurements allow performing a very refined tomography: knowing the expected emission wavelength of the line under study allows for a precise and fine redshift distribution determination. In addition, IM is able to cover large cosmological volumes with respect to resolved galaxy surveys, in a relatively fast and inexpensive way.

In this work we aim at characterizing the cross-correlation signal between IM and GWs, focusing on the IM of the neutral hydrogen (HI) from the proposed 21cm IM survey with the SKAO and on resolved GW events from the merger of BBHs as detected by the Einstein Telescope (ET) [64]. A cross-correlation signal is expected because both HI and GWs trace the cosmic density field. Crucially, as we will see, they do so in different ways depending on some underlying assumptions on both astrophysics and cosmology.

We then present a few possible applications by studying astrophysical and cosmological tests that can be performed through the $\text{GW} \times \text{IM}$ cross-correlation and forecast their potential when considering expected data from the SKAO and the ET.

Firstly, we investigate the possibility of calibrating the statistical redshift distribution of GW events thanks to the cross-correlation with IM. This idea relies on the fact that, while GWs are affected by a large redshift uncertainty (in case an electromagnetic counterpart is not available, such as for BBHs), the IM provides uniquely refined tomographic information on the observed signal. Since the HI is a good tracer of the LSS, by assuming that the BBH have astrophysical origin, we would expect them to highly cross-correlate with the LSS and, consequently, with the HI IM signal. This is a generally valid technique applicable when considering two tracers, one of which is characterized by much smaller redshift errors than the other; this was already addressed in several works in the literature (see e.g., references [61, 63, 65–76]). Here we investigate, to our knowledge for the first time, its potential as a method to obtain statistical redshift distributions for GW catalogs, which will provide a great improvement in dark sirens and cross-correlation studies.

Secondly, we study how this observable could help constraining cosmological models. As an example application, we focus on limits that will be possible to obtain for parameters describing the time evolution of the dark energy equation of state.

Thirdly, we tackle the issue of understanding the nature of the progenitors of the merging BBHs: evidences of the presence of Primordial Black Holes (PBHs) among the detected mergers can be found by looking at how GWs trace the underlying matter distribution (and, consequently, the HI IM signal) since different formation scenarios provide different predictions [38, 39].

This manuscript is structured as follows: in section 2 we present the methodology used, introducing the mathematical formalism for the cross-correlation angular power spectra and then the Fisher matrix we use for our analyses; in section 3 we characterize our GW and HI tracers; in section 4 we describe the GW statistical redshift distribution calibration application; in section 5 we address the dynamical DE topic; in section 6 we tackle the determination of the BBHs progenitors and in section 7 we draw our conclusions.

2 Methodology

In this section we introduce the mathematical formalism used in this work: in section 2.1 we characterize the angular power spectra C_ℓ s and then in section 2.2 we describe the methodology adopted for obtaining our results, namely the Fisher matrix formalism.

2.1 Angular power spectra

The most natural way to compute cross-correlations is by looking at the 3D angular power spectrum, C_ℓ , therefore calculating the correlation of distributions on concentric spheres. This formalism has a long history in cosmology and was initially developed in [77, 78], and subsequently applied to cosmological datasets in [79–82]; more recently it has been used mostly for cross-correlations (e.g., [22]). The advantage of this formalism resides in the fact that it naturally includes effects coming from large angular separations, the curvature of the sky, and that it makes use of directly observable quantities such as angles and redshifts. The drawback of having to calculate a large number of auto- and cross- bin correlations in the case of many narrow redshift bins does not apply here as we do not have very good radial information for the GW maps. Moreover, recent theoretical developments allow us to compute a large number of correlations in very short times (see [83, 84]).

In the following we describe the general formalism for this calculation for resolved events, such as in the cases of e.g., galaxies or GW events, where C_ℓ s indicate *number counts* angular power spectra. In section 3.2 we describe how this formalism can easily be extended to non-resolved tracers such as HI from intensity mapping.

Defining the number count fluctuations of a tracer X at redshift z and direction \hat{n} as $\delta^X(z, \hat{n})$, we can expand it in spherical harmonics $Y_{\ell m}(\hat{n})$ using the harmonic coefficients $a_{\ell m}^X(z)$, as

$$\delta^X(z, \hat{n}) = \sum_{\ell m} a_{\ell m}^X(z) Y_{\ell m}(\hat{n}). \quad (2.1)$$

The relation between the harmonic coefficients and the *observed* angular power spectrum $\tilde{C}_\ell^{XY}(z_i, z_j)$ (describing the cross-correlation of tracer X in redshift bin z_i with tracer Y in bin z_j) is the covariance of the coefficients of the spherical harmonics expansion, given by:

$$\langle a_{\ell m}^X(z_i) a_{\ell' m'}^{Y*}(z_j) \rangle = \delta_{\ell \ell'} \delta_{m m'} \tilde{C}_\ell^{XY}(z_i, z_j), \quad (2.2)$$

where δ stands for the Kronecker delta. Note that this expression is strictly valid only in the case of isotropic and homogeneous fields (see [85]). For the case of this paper, however, we

will continue using the standard formalism derived from equation (2.2) because of the poor angular and radial resolution of GW maps.

The $a_{\ell m}^X(z_i)$ coefficients are built from the partial wave coefficients of the signal and of the noise

$$a_{\ell m}^X(z_i) = s_{\ell m}^X(z_i) + n_{\ell m}^X(z_i). \quad (2.3)$$

The *observed* angular power spectrum is then written as

$$\tilde{C}_\ell^{XY}(z_i, z_j) = C_\ell^{XY}(z_i, z_j) + \mathcal{N}_\ell^{XY}(z_i, z_j). \quad (2.4)$$

The cross-correlation angular power spectrum of the signal and noise are computed from the signal wave coefficients as (see e.g. [77, 79–82, 86, 87])

$$\langle s_{\ell m}^X(z_i) s_{\ell' m'}^{Y*}(z_j) \rangle = \delta_{\ell\ell'} \delta_{mm'} C_\ell^{XY}(z_i, z_j) \quad (2.5)$$

$$\langle n_{\ell m}^X(z_i) n_{\ell' m'}^{Y*}(z_j) \rangle = \mathcal{N}_{\ell m}^{XY}(z_i, z_j). \quad (2.6)$$

For the GW detection we set up a SNR of 8 to guarantee detections and include a shot noise term, while we use a combination of instrumental and foreground noises for IM (see section 3 for details on their explicit expressions). We also assume that signal and noise are statistically independent, $\langle s_{\ell m}^X(z_i) n_{\ell' m'}^{Y*}(z_j) \rangle = 0$. The 3D angular power spectrum of tracers $\{X, Y\}$ at redshifts $\{z_i, z_j\}$ can be written as

$$C_\ell^{XY}(z_i, z_j) = \frac{2}{\pi} \int \frac{dk}{k} \mathcal{P}(k) \Delta_\ell^{X, z_i}(k) \Delta_\ell^{Y, z_j}(k), \quad (2.7)$$

where $\mathcal{P}(k) = k^3 P(k)$ is the primordial power spectrum and

$$\Delta_\ell^{X, z_i}(k) = \int_0^\infty dz \frac{dN_X}{dz} W(z, z_i, \Delta z_i) \Delta_\ell^X(k, z). \quad (2.8)$$

Here $W(z, z_i, \Delta z_i)$ are observational window functions related to the specific experiment centered at z_i with half-width Δz_i and $\frac{dN_X}{dz}$ stands for the source number density per redshift interval. Note that the integral of $W(z, z_i, \Delta z_i) \frac{dN_X}{dz}$ is normalized to unity. Finally, $\Delta_\ell^X(k, z)$ is the angular number count fluctuation of the X tracer, which is the sum of density (den), velocity (vel), lensing (len) and gravity (gr) effects [86, 87]:

$$\Delta_\ell^X(k, z) = \Delta_\ell^{\text{den}}(k, z) + \Delta_\ell^{\text{vel}}(k, z) + \Delta_\ell^{\text{len}}(k, z) + \Delta_\ell^{\text{gr}}(k, z). \quad (2.9)$$

The reader interested in the full expression of the terms in equation (2.9) can find them in appendix A. In this work we computed angular power spectra using `Multi_CLASS`¹, the modified version of `CLASS` [88, 89] presented in [90, 91] which allows to compute cross-correlations between different tracers.

In the following, we list and briefly describe the relevant physical quantities for the computation. More details about the specifics for the tracers considered in this work (redshift distributions, biases, redshift binning, etc.) are provided in sections 3.1 and 3.2.

¹Publicly available at https://github.com/nbellomo/Multi_CLASS.

- *Redshift distribution* $\frac{dN_X}{dz}$: observed source number density per redshift interval of tracer X . It appears in equation (2.8) for the $C_{\ell s}$ computation, in which its shape is the only significant feature, whereas its overall amplitude has no relevance due to the normalization. The total number of objects as a function of redshift is instead used when computing the shot noise of resolved sources. We have checked that using a top-hat or a gaussian window function does not significantly affect our findings.
- *Bias* b_X : it describes the relation between a given observable X and the underlying distribution of matter that it traces (see e.g., [92–99]). Considering the linear bias formulation and indicating the local contrasts of matter and tracer X at position x respectively by $\delta(x)$ and $\delta_X(x)$, the bias is defined as $\delta_X(x) \equiv \frac{n_X(x) - \bar{n}_X}{\bar{n}_X} = b_X \delta(x)$, where n_X is the comoving density of tracer X and \bar{n}_X is its mean value. This physical quantity is a linear factor in the density term of equation (2.9). In this work we will also make use of the quantity \bar{b}_X , which provides an average value of the bias of tracer X in a considered redshift range $[z_{\min}, z_{\max}]$, weighted for the tracer redshift evolution:

$$\bar{b}_X = \frac{\int_{z_{\min}}^{z_{\max}} dz b_X(z) \frac{d^2 N_X}{dz d\Omega}}{\int_{z_{\min}}^{z_{\max}} dz \frac{d^2 N_X}{dz d\Omega}} \quad (2.10)$$

with $X = \{\text{GW}, \text{IM}\}$. In this way, estimating a mean value for this parameter, we take into account which redshift interval (i.e. bias values) weights the most.

- *Magnification bias* $s_X(z)$: it quantifies how the observed surface density of sources of tracer X is influenced by gravitational lensing effects [100]. The observable result is given by the contribution of two opposite effects: whereas the number of observed sources can grow thanks to a magnification effect of the incoming flux, an increase of the area lowers the observed number density of objects. The magnification bias is a dominant term in the lensing contribution of equation (2.9), but affects also the velocity and gravity terms.
- *Evolution bias* f_X^{evo} : this term is present due to the fact that the *absolute* number of objects of a tracer X may not be conserved over time due to the possible formation of new objects. It reads as [101–103]: $f_X^{\text{evo}}(z) = \frac{d \ln \left(a^3 \frac{d^2 N_X}{dz d\Omega} \right)}{d \ln a}$, where a is the scale factor and $\frac{d^2 N_X}{dz d\Omega}$ is the absolute distribution of objects of tracer X , which in principle is not the same as the observed one introduced above. The evolution bias appears only in sub-leading contributions to equation (2.9).

We have already mentioned that the bias parameters introduced above come into play in quantifying the angular number count fluctuations of equation (2.9) (see appendix A for full expressions). In the following we explicitly summarize the dependence of each of the number counts contributions on the bias parameters ($b_X, s_X, f_X^{\text{evo}}$):

$$\begin{cases} \Delta_{\ell}^{\text{den}} = \Delta_{\ell}^{\text{den}}(b_X) \\ \Delta_{\ell}^{\text{vel}} = \Delta_{\ell}^{\text{vel}}(s_X, f_X^{\text{evo}}) \\ \Delta_{\ell}^{\text{len}} = \Delta_{\ell}^{\text{len}}(s_X) \\ \Delta_{\ell}^{\text{gr}} = \Delta_{\ell}^{\text{gr}}(s_X, f_X^{\text{evo}}) \end{cases} \quad (2.11)$$

where dependencies on k and z are implied.

2.2 Fisher analysis

In this work we make use of the Fisher analysis methodology, which we briefly sketch here to introduce the general formalism we adopt. Assuming GWs and IM signals as the two tracers, we divide the total redshift interval surveyed by considered GW experiments in $N_{\text{bins}}^{\text{GW}}$ bins, with amplitude Δz^{GW} , and the signal from intensity mapping distributed among $N_{\text{bins}}^{\text{IM}}$ redshift bins with amplitude Δz^{IM} .

Considering the observed power spectra \tilde{C}_ℓ s and a generic set of parameters $\{\theta_n\}$ for the Fisher analysis, we can organize our data in the (symmetric) matrix \mathcal{C}_ℓ as

$$\mathcal{C}_\ell = \begin{bmatrix} \tilde{C}_\ell^{\text{IMIM}}(z_1^{\text{IM}}, z_1^{\text{IM}}) & \dots & \tilde{C}_\ell^{\text{IMIM}}(z_1^{\text{IM}}, z_N^{\text{IM}}) & \tilde{C}_\ell^{\text{IMGW}}(z_1^{\text{IM}}, z_1^{\text{GW}}) & \dots & \tilde{C}_\ell^{\text{IMGW}}(z_1^{\text{IM}}, z_N^{\text{GW}}) \\ & & \dots & \tilde{C}_\ell^{\text{IMIM}}(z_2^{\text{IM}}, z_N^{\text{IM}}) & \tilde{C}_\ell^{\text{IMGW}}(z_2^{\text{IM}}, z_1^{\text{GW}}) & \dots & \tilde{C}_\ell^{\text{IMGW}}(z_2^{\text{IM}}, z_N^{\text{GW}}) \\ & & & \vdots & \vdots & & \vdots \\ & & \dots & \tilde{C}_\ell^{\text{IMIM}}(z_N^{\text{IM}}, z_N^{\text{IM}}) & \tilde{C}_\ell^{\text{IMGW}}(z_N^{\text{IM}}, z_1^{\text{GW}}) & \dots & \tilde{C}_\ell^{\text{IMGW}}(z_N^{\text{IM}}, z_N^{\text{GW}}) \\ & & & & \tilde{C}_\ell^{\text{GWGW}}(z_1^{\text{GW}}, z_1^{\text{GW}}) & \dots & \tilde{C}_\ell^{\text{GWGW}}(z_1^{\text{GW}}, z_N^{\text{GW}}) \\ & & & & & & \vdots \\ & & & & & \dots & \tilde{C}_\ell^{\text{GWGW}}(z_N^{\text{GW}}, z_N^{\text{GW}}) \end{bmatrix}, \quad (2.12)$$

The \mathcal{C}_ℓ matrix has dimensions of $(N_{\text{bins}}^{\text{IM}} + N_{\text{bins}}^{\text{GW}}) \times (N_{\text{bins}}^{\text{IM}} + N_{\text{bins}}^{\text{GW}})$. We remind the reader that the tilde symbol stands for *observed* \tilde{C}_ℓ s.

The \mathcal{C}_ℓ matrix is then used to compute the Fisher matrix elements as

$$F_{\alpha\beta} = f_{\text{sky}} \sum_{\ell} \frac{2\ell + 1}{2} \text{Tr} [\mathcal{C}_\ell^{-1} (\partial_\alpha \mathcal{C}_\ell) \mathcal{C}_\ell^{-1} (\partial_\beta \mathcal{C}_\ell)], \quad (2.13)$$

where ∂_α indicates the partial derivative with respect to the parameter θ_α and f_{sky} is the fraction of the sky covered by the intersection of IM and GW surveys. The sum over multipoles ℓ is performed up to a maximum value ℓ_{max} , which corresponds to the achievable angular resolution for the considered sources and instruments. For GW events an accurate estimate of ℓ_{max} would depend on (not limited to) redshift, SNR of the events and other source properties such as mass and spin. Since a rigorous analysis for the estimation of this parameter goes beyond the scope of this work, we use the constant threshold of $\ell_{\text{max}} = 100$, which provides a general plausible value for ET (as also performed in other studies, see e.g., [38–40]). All scales smaller than it are conservatively cut from the analysis.

Finally, the Fisher-estimated marginal error on the parameter θ_α is given by $\sqrt{(F^{-1})_{\alpha\alpha}}$. According to statistics and estimation theory, the so called Cramér-Rao bound provides the smallest error that one should expect to achieve in reality: errors on parameters deriving from “real-life” experiments are expected to be equal or higher than the Fisher estimated errors (Cramér-Rao inequality), where the equality stands only in the case of gaussian likelihood. Even though this is often an approximation and the Fisher approach may not always give precise results, it still remains an easy and quick method to provide forecasts for planned experiments.

3 Observables

In this section we characterize the considered tracers: resolved GWs from BBH mergers and the HI signal from intensity mapping experiments. In table 1 we summarize the redshift distributions for our tracers, as mentioned in sections 3.1 and 3.2.

Tracer	GW (ET)	IM (SKAO)
z range	[0.5-3.5]	
N_{bins}	3	30
Δz	1.0	0.1

Table 1. Chosen redshift specifics and experiments for the two tracers considered in this work. Note that the redshift ranges do not necessarily correspond to the best achievable from the indicated surveys.

3.1 Gravitational Waves

As first tracer we consider GWs from resolved mergers of BBHs, as detected by the Einstein Telescope (ET) experiment, as currently planned in [64]. We study this tracer for $N_{\text{bins}}^{\text{GW}} = 3$ redshift bins with width $\Delta z^{\text{GW}} = 1.0$ in the redshift range $[0.5 - 3.5]$. Even though the ET instrument would be able to detect BBH mergers outside this redshift range, we limit our analysis to it because it is the most optimal redshift range for the SKAO-Mid band IM survey (SKAO-MID) [14] (i.e., the survey we consider for our HI tracer). Considering GWs events beyond this limit would not help our analysis because we would not have any HI signal to cross-correlate them with.

It is worth noting that the ET is not the only planned third-generation GW detector. Another promising experiment is given by the Cosmic Explorer (CE) [104]. We anticipate here that, within our framework, results for ET and CE are quite similar, although slightly optimistic for the latter. We thus concentrate on the more conservative ET for the rest of the paper.

Note that we consider such large bins in order to take into account any possible luminosity distance uncertainty on the observed GWs events, also maintaining an approach as independent as possible on cosmological parameters. Indeed, the bin width $\Delta_z^{\text{GW}} = 1.0$ is larger than any redshift uncertainty estimated for LIGO/Virgo sources (see e.g., Table 6 of reference [4]), which will be even smaller for third-generation observatories. As a matter of fact, measurements of BBH mergers are associated to an uncertainty on the luminosity distance, which can be connected to a redshift uncertainty only by assuming a specific cosmology. An error on the assumed cosmology leads to a wrong assumption on the redshift of the event (and on its error). Since we are making use of a statistical tomographic approach, the main important element here is that the containing redshift bin for each observed event is the appropriate one. Assuming large bins for GWs makes this assumption safer, i.e., even when making errors on the assumed cosmology, the event-bin mapping would not be biased for most of the events. On the other hand, assuming smaller bins for GWs might provide more information and more optimistic forecasts, but it could lead to biased results if the wrong cosmology is assumed when actually performing these applications with real future data. We have tested the impact on our results on the bin width choice. As way of example, we found that by reducing Δ_z^{GW} from 1.0 to 0.5 (doubling the number of GW bins) the forecasts on the bias parameter \bar{b}_{GW} are 40% more optimistic, since a more refined tomographic information is being exploited. Nonetheless, this shows that results could be even more promising than those reported in this paper, but we preferred to choose a more conservative approach by adopting larger GW redshift bins, safely getting rid of any possible bias due to redshift or cosmology related errors. This makes the forecasts presented in this manuscript almost “cosmology-agnostic” and independent on reasonable errors on the single sources redshifts.

We characterize this tracer following prescriptions from references [40, 105], that we

summarize as:

- *Redshift distribution:* the redshift distribution of GWs events from BBHs mergers detected by the ET in the considered redshift range is taken from reference [105] and can be analytically interpolated in our redshift range as:

$$\frac{dN_{\text{GW}}}{dz} = Az^b \exp(-cz) \quad (3.1)$$

with $A = 0.825 \cdot 10^5$, $b = 2.40$, $c = 1.71$, assuming an observation time of $T_{\text{obs}}^{\text{GW}} = 1$ yr and $f_{\text{sky}} = 1$. Integrating this function with these specifics in our considered redshift range $0.5 < z < 3.5$ provides a total of $\sim 3.5 \cdot 10^4$ BBH mergers detections. Changes in $T_{\text{obs}}^{\text{GW}}$ and f_{sky} act simply as a re-scaling of the overall amplitude. The expression in equation (3.1) is obtained interpolating the results of the semi-analytical treatment of [105], in which galactic star formation rate functions, dependence of compact remnant masses on metallicity, time delays and stellar and binary evolution prescriptions are taken into account. Among astrophysical uncertainties, their findings are in agreement with other studies based on combining population synthesis simulations (e.g., [106–112]) with recipes on the cosmic Star Formation Rate (SFR) density and metallicity distributions inferred from observations (e.g., [113–118]). Finally, note that the BBH merger rate is normalized to a local value of $30 \text{ Gpc}^{-3}\text{yr}^{-1}$ at $z = 0$, in agreement with observed data from the first half of the LIGO/Virgo collaboration O3 run [119]. The normalized redshift distribution for GW events from astrophysical BBH mergers is provided in the left panel of figure 1.

- *Bias:* we make use of the findings of reference [40], in which the bias of GWs from BBH mergers is determined through an abundance matching technique (see e.g., [120]), associating the luminosity/SFR of the host galaxy to the mass of the hosting dark matter halo and then matching to a galaxy with given SFR the bias of the associated halo. Finally, characterizing BBH mergers with the same bias of their host galaxies, the final bias expression is obtained by taking into account which galaxy types proportionately contribute most to the detected merger rate. This quantity is provided in the central panel of figure 1 and can be interpolated up to $z \sim 3.5$ as:

$$b_{\text{GW}}(z) = a \exp(bz^d) + z^c \quad (3.2)$$

with $a = 0.948$, $b = -0.553$, $c = 0.996$, $d = 1.034$. The authors of reference [46] find a general agreement to the behaviour of these prescriptions, up to the redshift range considered in this work. Note that this determination of the bias, as well as the dN/dz , may also depend on other important astrophysical parameters, such as IMF and metallicity, and on the considered merging channel, such as isolated binaries, dynamical merger in stellar and nuclear stars clusters, mergers of PopIII stars, etc. References [40, 105], on which our assumptions are based, do not take into account merging efficiency dependencies on metallicity or IMF variations, and consider an isolated binaries merging channel. A more technical treatment of these quantities is beyond the scope of this work.

- *Magnification bias:* this quantity is defined as the logarithmic slope of the redshift distribution of detected events computed at detectability limit $\rho = \bar{\rho}$:

$$s_{\text{GW}}(z) = - \left. \frac{d \log_{10} \left(\frac{d^2 N_{\text{GW}}(z, > \rho)}{dz d\Omega} \right)}{d\rho} \right|_{\rho = \bar{\rho}}, \quad (3.3)$$

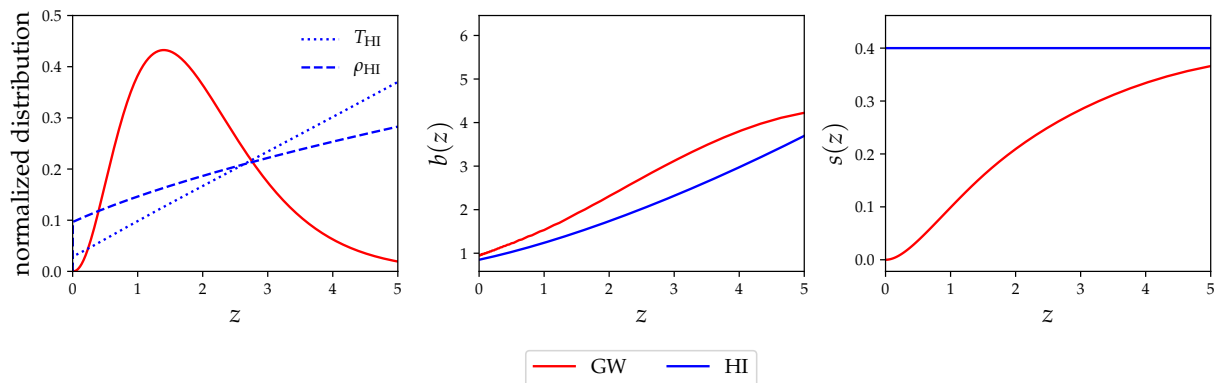


Figure 1. Specifics for the astrophysical GW and HI tracers considered in this work. *Left:* normalized redshift dependence (dN/dz for GWs; $T_b(z)$ and $\rho_{\text{HI}}(z)$ for HI). *Center:* bias $b(z)$. *Right:* magnification bias $s(z)$.

where ρ is the Signal-to-Noise ratio for each GWs event. Usually, detection of a GWs signal is considered solid for $\rho > \bar{\rho} = 8$. The magnification bias obtained from [40], and used in this work, is plotted in the right panel of figure 1.

- *Evolution bias:* by definition, the evolution bias for GWs events is straightforwardly given by

$$f_{\text{GW}}^{\text{evo}}(z) = \frac{d \ln \left(a^3 \frac{d^2 N_{\text{GW}}(z)}{dz d\Omega} \right)}{d \ln a}. \quad (3.4)$$

In figure 1 we provide redshift distribution and biases values for our GW tracer of astrophysical origin, together with the same quantities characterizing the HI from IM.

Noise sources

We characterize the considered GWs events with a shot-noise component as the only noise source to the angular power spectra:

$$C_\ell^{\text{N,GW}}(z_i, z_j) = C_\ell^{\text{shot}}(z_i, z_j) = \frac{\delta_{ij}}{\bar{n}(z_i)} \quad (3.5)$$

where δ_{ij} is the Kronecker delta and $\bar{n}(z_i)$ is the mean number density of sources in the i^{th} redshift bin. It affects the $C_\ell(z_i, z_i)^{\text{GW,GW}}$ entries (i.e. only cross-correlations between the same GW tracer among the same redshift bin).

3.2 HI Intensity Mapping

In this section we characterize our second tracer: the forecasted measure of the HI distribution by a SKAO Mid-band (SKAO-MID) intensity mapping survey [14, 15, 121]. In the following sections we describe how the resolved sources formalism for the angular power spectra can be easily translated to be applied to the unresolved HI IM case, and we characterize the specifics for this observable.

Throughout this work we consider the HI tracer in the redshift range $[0.5 - 3.5]$, divided in bins of width $\Delta z^{\text{IM}} = 0.1$, for a total of $N_{\text{bins}}^{\text{IM}} = 30$ redshift bins. This is expected to be around the optimal redshift range for the SKAO-MID survey [14].

3.2.1 From resolved sources to IM

As provided in section 2.1, the cross-correlation formalism for resolved sources of different tracers is well defined and comprehensive of relativistic effects. When working with the IM signal of any line (the HI in our case), we do not deal with number counts, since we are looking at the ensemble of unresolved sources. However, the unresolved tracer case can be treated adapting the same formalism (e.g., [52, 122]). The following points are specifically referred to the HI, but are valid for any other line. In particular:

- *Redshift distribution*: while we characterize resolved sources with a redshift distribution of their number counts dN_X/dz , for the HI intensity mapping case we shall consider the HI comoving density distribution defined in [123] as $\rho_{\text{HI}}(z) = \Omega_{\text{HI}}(z)\rho_{\text{crit},0}$ and the mean brightness temperature $T_b(z)$. Their explicit expressions are (see e.g., [123, 124]):

$$\rho_{\text{HI}}(z) = 4(1+z)^{0.6}10^{-4} \cdot \rho_{\text{crit},0} \quad (3.6)$$

$$T_b(z) = 44\mu\text{K} \left(\frac{\Omega_{\text{HI}}(z)h}{2.45 \times 10^{-4}} \right) \frac{(1+z)^2}{E(z)}, \quad (3.7)$$

where $\rho_{\text{crit},0}$ is the critical density today and $E(z) = H(z)/H_0$. Since the density ρ_{HI} provides the redshift dependence of the *absolute* redshift distribution of HI atoms, whereas the mean brightness temperature T_b is a directly *observed* physical quantity through IM, we make use of T_b in place of the observed redshift distribution of equation (2.8) and of ρ_{HI} to compute the evolution bias term $f_{\text{evo}}(z)$. Both $\rho_{\text{HI}}(z)$ and T_b redshift dependencies are plotted in the left panel of figure 1.

- *Bias*: we can treat the bias analogously as it is done for the resolved sources case. In this work we use the following analytic expression obtained fitting results from reference [125]:

$$b_{\text{HI}}(z) = a(1+z)^b + c, \quad (3.8)$$

with $a = 0.22$, $b = 1.47$ and $c = 0.63$. This quantity is plotted in the central panel of figure 1. This prescription originates from the outputs of a semi-analytical model for galaxy formation that include an explicit treatment of neutral hydrogen and are in agreement with the findings of [126] based on Illustris TNG hydro-dynamical simulations. The bias is expected to be around unity at low z (e.g. ~ 0.85 at $z \sim 0.06$ [127]), where the HI is strongly present in young galaxies with high Star Formation Rates [8]. In order to make sure that uncertainties on the HI bias at higher z do not affect the conclusions of our work, we have checked that performing the same analysis with the extreme hypothesis of a constant unitary value of $b_{\text{HI}}(z)$ leads to a change on the Fisher estimated errors for cosmological parameters below 15%.

- *Magnification bias*: when treating any IM experiment, the magnification bias assumes the value

$$s_{\text{HI}}(z) = 0.4, \quad (3.9)$$

which corresponds to the absence of lensing effects. This is due to the fact that the observed physical quantity is a surface brightness (instead of number counts) which is not altered by this type of phenomena (see e.g., [122] and references therein).

- *Evolution bias*: as mentioned above, this quantity is obtained analogously to the resolved sources case, substituting the redshift distribution for resolved sources with the density distribution:

$$f_{\text{HI}}^{\text{evo}}(z) = \frac{d \ln \rho_{\text{HI}}(z)}{d \ln a} \quad (3.10)$$

with a being the scale factor.

3.2.2 Noise sources

When considering C_ℓ s including the IM component (both IM \times IM and GW \times IM cases) we express the relation between theoretical C_ℓ^{XY} (computed with `Multi_CLASS`) and the observed \tilde{C}_ℓ^{XY} as:

$$\tilde{C}_\ell^{\text{IM,IM}}(z_i, z_j) = \mathcal{B}(z_i)\mathcal{B}(z_j)C_\ell^{\text{IM,IM}}(z_i, z_j) + C_\ell^{\text{N,IM}} \quad (3.11)$$

and

$$\tilde{C}_\ell^{\text{IM,GW}}(z_i, z_j) = \mathcal{B}(z_i)C_\ell^{\text{IM,GW}}(z_i, z_j) \quad (3.12)$$

where the $\mathcal{B}^X(z_i)$ encodes the signal suppression at scales smaller of the FWHM of the beam θ_B . In single-dish configuration $\theta_B \sim 1.22\lambda/D_d$, thus implying a more severe suppression of the signal at lower frequencies:

$$\mathcal{B}(z_i) = \exp[-\ell(\ell+1)(\theta_B(z_i)/\sqrt{16 \ln 2})^2]. \quad (3.13)$$

In equation (3.11), the term $C_\ell^{\text{N,IM}}$ indicates noise sources (see also equation (2.4)). For the HI case we consider the intrinsic noise of the instrument C_ℓ^{instr} and the residual error due to the procedure of cleaning the cosmic IM signal from the bright foreground emission C_ℓ^{fg} :

$$C_\ell^{\text{N,IM}} = C_\ell^{\text{instr}} + C_\ell^{\text{fg}}, \quad (3.14)$$

whereas the shot-noise is instead a very subdominant component (see e.g., [126, 128]). In the following paragraphs we describe how these noise sources are treated.

Instrumental noise

The experiment setup considered in this work is IM performed in single dish [12, 14] mode and with a collection of N_d dishes. The noise angular power spectrum for this case is given by (see e.g., [12, 16, 129]):

$$C_\ell^{\text{instr}} = \sigma_T^2 \theta_B^2. \quad (3.15)$$

The single-dish rms noise temperature σ_T writes as

$$\sigma_T \approx \frac{T_{\text{sys}}}{\sqrt{n_{\text{pol}} B t_{\text{obs}}}} \frac{\lambda^2}{\theta_B^2 A_e} \sqrt{S_{\text{area}}/\theta_B^2} \sqrt{\frac{1}{N_d}}. \quad (3.16)$$

Since the beam FWHM of a single dish is $\theta_B \sim 1.22\lambda/D_d$, one gets $\lambda^2/A_e \sim \lambda^2/D_d^2 \sim \theta_B^2$, where D_d is the diameter of a single dish, A_e is the effective collecting area of the dish and $\lambda = \lambda(z)$ is the observed wavelength of the redshifted 21cm signal emitted at z : $\lambda(z) = \lambda_{21\text{cm}}(1+z)$. From this, one can write:

$$C_\ell^{\text{instr}}(z_i) \approx \left(\frac{T_{\text{sys}}}{T_b(z_i) \sqrt{n_{\text{pol}} B t_{\text{obs}} N_d}} \sqrt{\frac{S_{\text{area}}}{\theta_B^2}} \frac{1}{T_b(z_i)} \right)^2 \theta_B^2. \quad (3.17)$$

Following SKAO-MID prescriptions, we have the following parameters values: $T_{\text{sys}} = 28K$ for the system temperature, $B = 20 \cdot 10^6 Hz$ for the bandwidth, $t_0 = 5000h = 1.8 \cdot 10^7 s$ for the observation time, $N_d = 254$ for the total number of dishes, $S_{\text{area}} = 20000 deg^2$ for the total surveyed area, $A_e = 140m^2$ and $D_d = 15m$. Notice the normalization to the mean brightness temperature at the center of the redshift bin $T_b(z_i)$, needed to retrieve a dimensionless power spectrum to be added to the theoretical dimensionless one in order to estimate the observed $C_{\ell s}$, according to equation (2.4). Numerical values are taken from table 2 of reference [16]. Even though $S_{\text{area}} = 20000 deg^2 \sim f_{\text{sky}} = 0.5$ is the official expected value of sky coverage, for the purpose of this work we consider also different values of f_{sky} .

Finally, we remark that the $C_{\ell}^{\text{instr}}(z_i)$ noise component is expressed as function of one single redshift because we assume that it is de-correlated among different bins, affecting only auto-correlations.

Foregrounds

The presence of strong foregrounds is one of the central challenges of IM, currently preventing a detection in auto-correlation of the signal (see e.g., references [130, 131]). Such detection should instead be possible for an IM survey with SKAO telescope due to improvements in the signal-to-noise, to a larger scanned sky patch and to the larger frequency band. Nevertheless, the cleaning procedure will not be perfect and the recovery of the pristine HI signal will still be partially complicated by the foreground emission. This effect has been studied with simulations with various degrees of complexity [132–136]. For the purposes of this work, we quantify the residual error that could be expected after a foregrounds removal procedure adding a noise term C_{ℓ}^{fg} to the theoretical $C_{\ell s}$, for the IM \times IM components and for any redshift bins combination. Note that, since we focus on the angular power spectrum, we do not model the well known foreground cleaning effect of removing too much power at large scales along the line-of-sight. Our noise term is only a residual systematic accounting for the difficulties in cleaning large spatial scales. We model the C_{ℓ}^{fg} term as

$$C_{\ell}^{\text{fg}} = K^{\text{fg}} \cdot F(\ell), \quad (3.18)$$

where K^{fg} is a normalization constant determining the overall amplitude of the residual foregrounds related errors and $F(\ell)$ encodes the scale-dependency. We write this term as

$$F(\ell) = \frac{1}{f_{\text{sky}}} A e^{b\ell^c}, \quad (3.19)$$

accounting for a larger effect of the cleaning of the signal at larger scales and simply fitting this expression to results of [132] (middle-left panel of their figure 3), obtaining $A \sim 0.129$, $b \sim -0.081$, $c \sim 0.581$. This procedure introduces an error of around 12% at $\ell \sim 2$ and 4% at $\ell \sim 100$ (for $f_{\text{sky}} = 1.0$). It is also possible to define the variance of this systematic error (see e.g., [137]):

$$\sigma_{\text{sys}}^2 = \int \frac{d \ln \ell}{2\pi} \ell(\ell + 1) \left| C_{\ell}^{\text{fg}} \right|. \quad (3.20)$$

Setting the value of the overall normalization factor K^{fg} to an average value of all the $C_{\ell}^{\text{IM,IM}}(z_i, z_j)$ components:

$$K^{\text{fg}} = \left\langle C_{\ell}^{\text{IM,IM}}(z_i, z_j) \right\rangle, \quad (3.21)$$

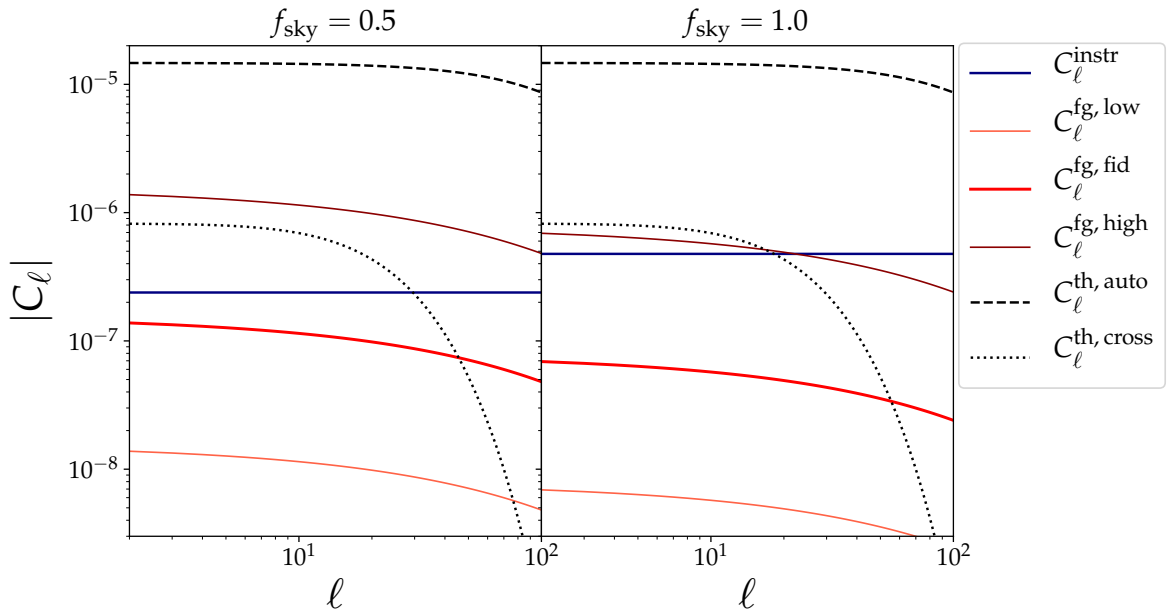


Figure 2. Comparison between HI angular power spectra C_ℓ s. In black: theoretical power spectra C_ℓ^{th} from `Multi_CLASS` for the $\text{IM} \times \text{IM}$ case, auto-correlating the 20th redshift bin ($2.4 < z < 2.5$) with itself (dashed line) and cross-correlating the 15th redshift bin ($1.9 < z < 2.0$) with the 20th (dotted line), as exemplificative case. In blue: instrumental noise power spectrum for SKAO-MID survey at redshift $z_{\text{mean}} = 2.5$. In different shades of red: foreground cleaning noise power spectra, with amplitudes equal to K^{fg} ($C_\ell^{\text{fg, fid}}$), $0.1 \cdot K^{\text{fg}}$ ($C_\ell^{\text{fg, low}}$) and $10 \cdot K^{\text{fg}}$ ($C_\ell^{\text{fg, high}}$). Left(right) panel corresponds to $f_{\text{sky}} = 0.5(1.0)$.

and considering our redshift binning, we obtain a fiducial value of

$$K^{\text{fg}} \simeq 6 \cdot 10^{-7}. \quad (3.22)$$

This leads to a variance of $\sigma_{\text{sys}}^2 \simeq 3 \cdot 10^{-7}$, in agreement with what assumed in [137].

In figure 2 we compare the resulting C_ℓ^{fg} for different amplitudes K^{fg} to the contribution from instrumental noise (at $z = 2.5$ by way of example). The contamination term from foreground removal is always dominant and stronger at low multipoles. We report in the figure also an example of the auto angular power spectrum of the HI signal and a cross power spectrum between two different bins.

We have repeated our analysis using different forms for (3.19) and with different amplitudes, and found a change in the Fisher estimated errors always below $\sim 10 - 15\%$. Therefore, this would not alter the conclusions reached. Note that our residual foreground contribution is neither frequency dependent nor considers possible coupling between the different scales. These should be secondary effects, especially assuming a full sky survey and a blind cleaning approach to cleaning [132, 138].

4 Gravitational waves statistical redshift distribution

The first application of the $\text{GW} \times \text{IM}$ cross-correlation we present in this work is the possibility to obtain a statistical determination of the redshift distribution of GWs detected by laser

interferometers. Those detections in fact provide information only on the chirp mass of the system and the (GW) luminosity distance, therefore redshift information is only a derived quantity, based on astrophysical and cosmological assumptions [139, 140]. We rely on the idea that a given tracer whose redshift distribution is well defined can help in calibrating that of a second tracer through studying the cross-correlation of the two. This was already done in several works with techniques such as correlations or the so-called Clustering Based Redshift estimation (see e.g., [48, 53, 61, 63, 65–76, 141]). We mainly follow the methodology of reference [61], in which the authors perform a redshift calibration of a photometric sample of galaxies through cross-correlation with a spectroscopic sample.

Our case is equivalent, but we make use of the IM of the HI to calibrate GWs events. In fact, GW detected events are characterized by a big uncertainty on their localization due to poor angular resolution, whereas IM provides a refined sliced redshift information about the line under study. Assuming the progenitors of the merging BBHs have astrophysical origin, they are expected to trace very well the underlying distribution of the LSS, which is also well traced by the HI distribution. Combining these two tracers together is expected to improve the redshift localization of the poorly known one (GW) thanks to the refined information coming from other, much better localized (IM). We stress the fact that performing this analysis with resolved photometric galaxy samples instead of IM would not be feasible, due to their lower redshift resolution.

Let us stress again that this methodology aims at calibrating the statistical distribution of a tracer which is poorly localized: this is why we only consider BHBH mergers without taking into account also Neutron Stars (NS) binaries or BHNS systems. Indeed, these latter types of systems can likely be matched to an electromagnetic counterpart, allowing for a well precise localization of the binaries, much more competitively than what the method explored in this section can accomplish.

Given our fiducial redshift distribution for GWs (as described in section 3.1), we re-model it as a piecewise (PW) function. Each piece has width equal to the IM bin width Δz^{IM} , so that the total number of pieces is equal to $N_{\text{bins}}^{\text{IM}} = 30$ and each of them perfectly overlaps with a specific IM redshift bin. The overall amplitude of the PW function in the i^{th} bin is indicated as A_i .

Following the formalism described in section 2.2, we perform a Fisher matrix analysis considering the following set of Fisher parameters: the 30 amplitudes $\{A_i\}$ of the GWs PW redshift distribution and $\{\ln 10^{10} A_s, n_s, \bar{b}_{\text{GW}}, \bar{b}_{\text{HI}}, K^{\text{fg}}\}$ (for a total of 35 parameters)². The spectral index and amplitude n_s and A_s are introduced in the pipeline in order to account for a possible cosmology dependence of our results. A fully cosmology based pipeline (including also the dark energy parameters $\{w_0, w_a\}$) will be explored in section 5. We set Planck priors on $\{\ln 10^{10} A_s, n_s\}$ [142].

Note that there is a disadvantage in performing $\text{GW} \times \text{IM}$ instead of $\text{LSS} \times \text{IM}$ (such as in reference [61]) and constraining the GWs redshift distribution is more difficult than that of photometric galaxy samples. Firstly, the sum over multipoles of equation 2.13 stops at $\ell_{\text{max}} = 100$ (for ET), while galaxy surveys provide a much higher angular resolution (e.g., $\ell_{\text{max}} \sim 2000$ in [61]). Also, less objects are detected when considering GWs signals from

²The fiducial parameters values we use in this pipeline are: $\{\ln 10^{10} A_s, n_s, \bar{b}_{\text{GW}}, \bar{b}_{\text{HI}}, K^{\text{fg}}\} = \{3.098, 0.9619, 2.166, 1.851, 6 \cdot 10^{-7}\}$. The cosmology parameters values are taken from Planck [142], the biases values are obtained applying equation (2.10) in the considered redshift range $[0.5, 3.5]$ and the K^{fg} value derives from equation (3.22). Finally, the fiducial values for the amplitudes $\{A_i\}$ are given by the amplitudes of the full GWs redshift distribution at the corresponding redshifts.

BHBH mergers, inducing a more relevant shot noise contribution, which is translated into higher error bars.

From the Fisher estimated error σ_{A_i} on the amplitudes A_i one can directly compute a relative error given by the fraction between the error and the fiducial value A_i :

$$e_{A_i}^{\text{rel}} = \sigma_{A_i}/A_i. \quad (4.1)$$

In figure 3 we show the error bars on the 30 GW redshift distribution amplitudes A_i with absolute errors (left panels) and relative errors (right panels) for various combinations of $T_{\text{obs}}^{\text{GW}}$ and f_{sky} . We recall that the $f_{\text{sky}} = 0.5$ value is the fiducial scenario for SKAO-MID, whereas cases for lower values of f_{sky} can be considered conservative, and higher values can be thought as a limiting case for future experiments. It is possible to see that for enough high values of $T_{\text{obs}}^{\text{GW}}$ and f_{sky} the error-bars are relatively small and the relative error is below unity. This takes place mainly at lower redshifts, whereas increasing z the error size becomes large and the relative error is raised above unity. Overall, it is possible to see that redshift calibration of GWs events is quite effective in the low-medium redshift range, whereas at higher redshift very high values of $T_{\text{obs}}^{\text{GW}}$ and f_{sky} would be required, when possible.

We conclude noting one fundamental peculiarity of our approach, which is basically “cosmology-agnostic”, in the sense that it solely relies on the cross-correlations between GWs (in large z bins, to account for redshift localization uncertainties) and IM (in appropriately small bins). It is independent from the underlying “true” cosmology, since we have only assumed fiducial cosmological parameters to perform our Fisher forecasts, but no assumptions in this regards will be needed when working with actual data (thanks to the large width of the considered GWs redshift bins). In addition, note also that in our Fisher analysis we allow for variation of the 30 amplitudes on the GWs redshift distribution: this essentially corresponds to not imposing any prior on the shape of this distribution, taking out any astrophysical assumption that would have imprints on the distribution shape. Forecasts obtained in this way are more pessimistic than other works in current literature (see e.g., [143]) and this is due to the fact that a very general approach is being taken here, without any cosmology/astrophysics priors. Finally, let us stress again that the aim of this application is to calibrate the *statistical* distribution of GWs sources, i.e., improving the knowledge on the disposition along redshift of the whole ensemble. We do not aim at better localizing each single event. For this reason, we do not need to take into account the redshift error of each source, as long as the GW redshift binning is large enough the compensate any possible uncertainty in this regard.

5 Cosmological constraints: dynamical dark energy

The $\text{GW} \times \text{LSS}$ cross-correlation, as a tracer of the matter density field, can provide information on a variety of cosmological parameters. Regarding the $\text{GW} \times \text{IM}$ observable, given the specific redshift range and peculiarities of the expected signal, there might be some particular model or parameter that will be optimally tested by it.

In this section we present an example of one of such measurements, which is the possibility of constraining dark energy parameters; in particular, we will focus on parameters describing the redshift evolution of its equation of state.

Starting from the Einstein field equations, which describe how gravity behaves due to the presence of mass-energy (and how this moves given the space-time curvature), one can write

$$G_{\mu\nu} = T_{\mu\nu}, \quad (5.1)$$

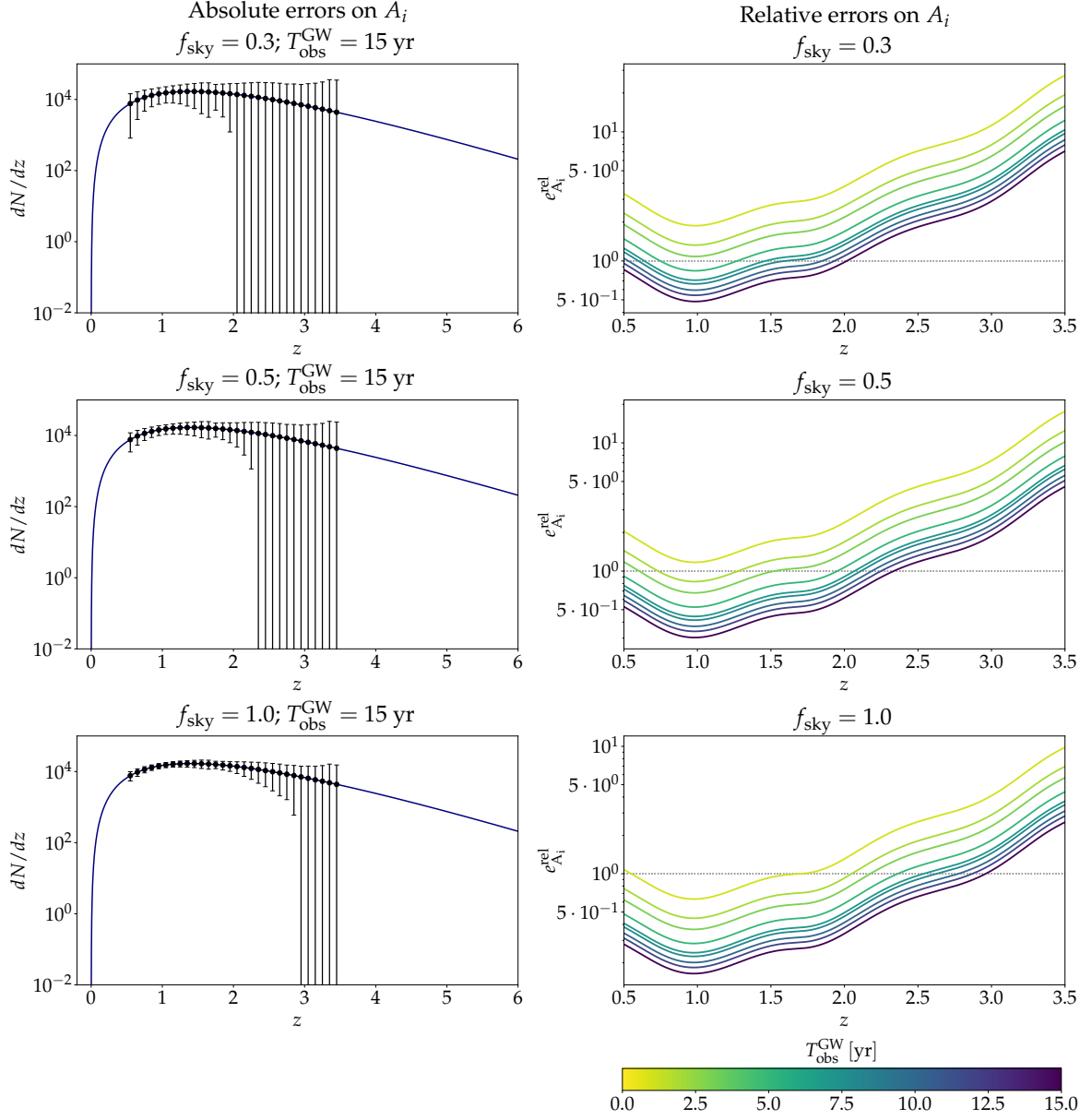


Figure 3. *Left:* GW fiducial redshift distribution (in blue) with error-bars on the amplitude parameters A_i . *Right:* Fisher estimated relative errors $e_{A_i}^{\text{rel}}$ on the amplitude parameters A_i . Different values of $T_{\text{obs}}^{\text{GW}}$ (from 1 yr to 15 yr) and f_{sky} ($f_{\text{sky}} = 0.3, 0.5, 1.0$) are provided.

with the appropriate choice of conventions. Here $G_{\mu\nu}$ and $T_{\mu\nu}$ are the so called Einstein tensor and stress-energy tensor respectively. In order to account for the observed accelerated expansion of the Universe, in a General Relativistic framework, equations (5.1) have to be modified substituting $T_{\mu\nu}$ with $T'_{\mu\nu} = T_{\mu\nu} + T_{\mu\nu}^{\text{DE}}$, where $T_{\mu\nu}^{\text{DE}} = -\Lambda g_{\mu\nu}$ (with $g_{\mu\nu}$ the metric tensor) and DE stays for dark energy. This can be in the form of a cosmological constant or an additional field. Among the many possible proposed models and deviations from the cosmological constant (originally inspired by vacuum energy), a possibility is to investigate deviations from its equation of state (eos) being constant with redshift. The eos is defined as $w = \frac{p}{\rho}$ (where p and ρ are respectively the pressure and energy densities of the fluid). If the DE behaviour is described by a cosmological constant, then $w = -1$, whereas the relation

$$w(a) = w_0 + w_a(1 - a) \quad (5.2)$$

generally describes the case of time evolution. Current measurements from CMB and galaxy clustering are consistent with a cosmological constant [144, 145], but many models predict small departures from the cc case (see e.g., [146, 147]), therefore this remains an important part in the efforts toward a better understanding of the cosmological model.

Here we investigate how well the DE parameters $\{w_0, w_a\}$ can be constrained through GW \times IM cross-correlations. We include in our Fisher analysis pipeline summarized in section 2.2 the following parameters: $\{w_0, w_a, \omega_{\text{cdm}}, \omega_{\text{b}}, 100\theta_s, \ln 10^{10} A_s, n_s, \bar{b}_{\text{GW}}, \bar{b}_{\text{HI}}, K^{\text{fg}}\}$ (for a total of 10 parameters)³. The differences with respect to the analysis of section 4 consist in the usage of the full GWs redshift distribution (in place of its piece-wise approximation) and the addition of other cosmology related Fisher parameters: w_0, w_a , the cold dark matter physical density $\omega_{\text{cdm}} = \Omega_{\text{cdm}} h^2$, the baryon physical density $\omega_{\text{b}} = \Omega_{\text{b}} h^2$ and the angular scale of the sound horizon at decoupling $100\theta_s$. We set a Planck prior on the $\{\omega_{\text{cdm}}, \omega_{\text{b}}, 100\theta_s, \ln 10^{10} A_s, n_s\}$ parameters, unless where stated otherwise.

In figure 4 we provide forecasts for the constraining power on the dark energy parameters $\{w_0, w_a\}$ for the experiments considered in this work, including or not Planck priors and for different values of f_{sky} . On the right panel we can see the improvement that would come by increasing the fraction of the sky surveyed. Overall, we can notice that the predicted constraints are qualitatively in agreement with other studies, such as e.g., reference [148] in which a study of the cross-correlation between GWs and radio galaxy surveys is performed or reference [129] in which forecasts are obtained for HI intensity mapping experiments.

We can also see that constraints are approximately comparable to the BOSS+Planck results available in the literature (see e.g., [145]) for what concerns the errors on the $\{w_0, w_a\}$ parameters, with w_0 constraints slightly weaker. Comparing our results with those from the Euclid collaboration, we can see that (see e.g., [149]) our constraints are approximately comparable or slightly less competitive when considering combinations of all probes tested by Euclid (weak lensing and spectroscopic/photometric galaxy clustering), but more stringent with respect to Euclid forecasts obtained through one single probe. A similar comparison can be done when looking at forecasts for the Vera Rubin Observatory (LSST, see e.g., [150]): our forecasts are more optimistic than those from the LSST (up to 50%) when considering just the single isolated probes testable by the survey, but become less competitive when their

³The fiducial parameters values we use in this pipeline are: $\{w_0, w_a, \omega_{\text{cdm}}, \omega_{\text{b}}, 100\theta_s, \ln 10^{10} A_s, n_s, \bar{b}_{\text{GW}}, \bar{b}_{\text{HI}}, K^{\text{fg}}\} = \{-1.0, 0.0, 0.12038, 0.022032, 1.042143, 3.098, 0.9619, 2.166, 1.851, 6 \cdot 10^{-7}\}$. As in the previous section, the cosmology parameters values are taken from Planck [142], the biases values are obtained applying equation (2.10) in the considered redshift range [0.5, 3.5] and the K^{fg} value derives from equation (3.22).

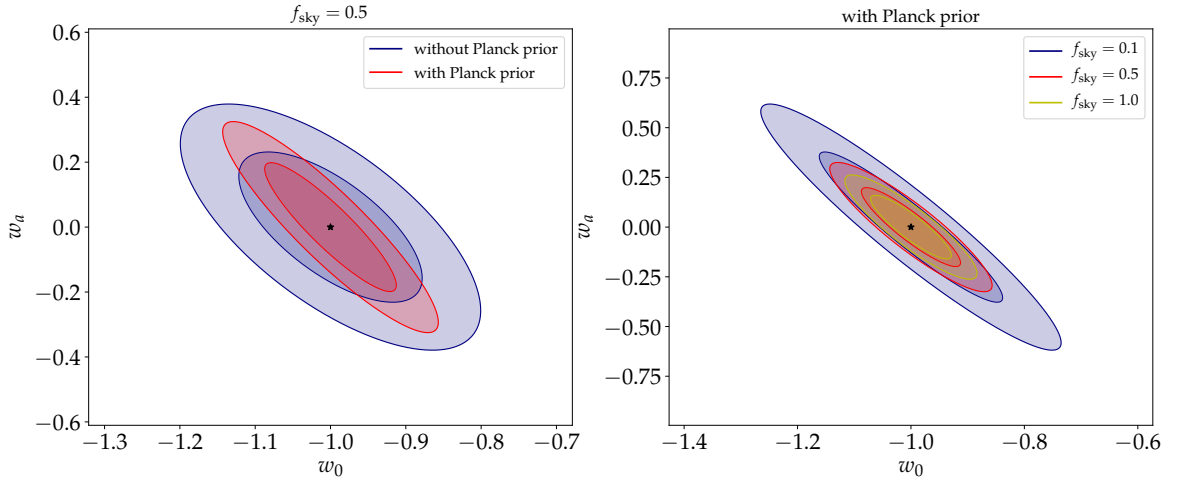


Figure 4. Contour plots for the DE parameters $\{w_0, w_a\}$ at 1σ and 2σ confidence levels, for fixed $T_{\text{obs}}^{\text{GW}} = 10\text{yr}$. *Left:* forecasts for fixed $f_{\text{sky}} = 0.5$. With and without applying a Planck prior on other cosmology parameters. *Right:* forecasts for different values of f_{sky} (as legend). A Planck prior on all other cosmology parameters is applied.

combination in the LSST is exploited. All in all, although the forecasts we obtain with this methodology are not competitive with the maximum potential that other surveys (such as those mentioned above) can achieve, they can still provide an alternative way to test these scenarios. Cross-correlations are well known for helping in reducing systematics (see e.g., [151]). For this reason, these measurements will provide a very useful cross-check to available results, as they will come from cross-correlating two very different datasets and will be affected by much less and different systematics.

6 Astrophysical vs. primordial origin of merging black hole binaries

In this section we tackle the issue of using $\text{GW} \times \text{IM}$ for determining the origin of the progenitors of merging BBHs, distinguishing between the possibility that they originate from the end-point of stellar evolution, or that they are Primordial Black Holes (PBHs) generated in the early universe.

PBHs were first theorized a few decades ago [152, 153] when it was proposed that some over-dense regions in the primordial universe could reach the threshold for gravitational collapse and, in some regions, form black holes. Several formation mechanisms have been proposed in literature, such as the collapse of cosmic string loops or domain walls [154–158], the collapse of large fluctuations at inflation [159–161], bubble collisions [162, 163], but the mainstream hypothesis is that they originate from large perturbations in the primordial curvature power spectrum (that went outside of the horizon during inflation) right after horizon re-entry; there has been an intense activity in the community in the last few years on the relation between the primordial power spectrum and PBHs (see e.g., [164–176]).

The interest towards this type of compact objects revived after the first detection of GWs from the merger of two massive black holes [1, 2], when it was proposed that their progenitors might have primordial origin and even constitute a non negligible fraction of the dark matter, reviving the “PBHs as dark matter” hypothesis (e.g., [177, 178]). There is still no conclusive

agreement on the possibility that stellar-mass PBHs exist in sufficient abundance to make up for a considerable part of the dark matter (see e.g., [179–186] for some studies and constraints in this mass range), but confirmation (or exclusion) of their sheer existence would represent a big step in our understanding of the Universe. In fact, detecting even one PBH would provide invaluable information on the physics of the early Universe on scales otherwise inaccessible to standard cosmological measurements; moreover, it was recently shown that PBHs and WIMP DM are incompatible [187], so that the observation of one PBH would rule out the main DM candidate model.

Therefore, it will be extremely important to add another probe for the possible detection of the presence of PBHs and to understand their formation channels and merger rates. Measurements of GW \times IM will then add further information on this issue, on redshift ranges and with data sets complementary to what is and will be available otherwise. We refer the reader to PBH reviews such as e.g., [188–192] for more details.

The idea on top of which we build for our study follows the same logic of references [38, 39]: approaching the problem in a statistical way, we know that GWs from merging BBHs trace the underlying matter distribution in ways that depend on their origin (see later for more details) and consequently would correlate with the LSS - and the HI distribution, which is a tracer of the LSS - in different ways.

The relation between observables and the underlying matter distribution is encapsulated in the bias parameter introduced in section 2.1. Crucially, it has been shown [177, 184] that PBH mergers trace halos and the stellar distributions in ways that are different from endpoint of stellar evolution BHs, and in different ways depending on the PBH binary formation mechanism. This will then assign a different preferred bias \bar{b}_{GW} for the GWs, which will be the discriminant we can use for our study. The main features of the scenarios we aim to distinguish through GW \times IM are sketched in the following section.

6.1 Progenitors

In this section we briefly characterize the scenarios (astrophysical and different primordial ones) that we compare. To do so, we introduce the Γ_{pbh} parameter, which indicates the fraction of detected merging BBHs with primordial origin (over the total number of observed BBH mergers). Assuming the detection of \mathcal{N}_{tot} mergers, of which $\mathcal{N}_{\text{astro}}$ have astrophysical origin and \mathcal{N}_{pbh} have primordial origin ($\mathcal{N}_{\text{tot}} = \mathcal{N}_{\text{astro}} + \mathcal{N}_{\text{pbh}}$), the Γ_{pbh} parameter is defined as:

$$\Gamma_{\text{pbh}} = \mathcal{N}_{\text{pbh}} / \mathcal{N}_{\text{tot}} \quad (6.1)$$

and spans from $\Gamma_{\text{pbh}} = 0$ (i.e., only astrophysical BBH mergers are detected) to $\Gamma_{\text{pbh}} = 1$ (i.e., only primordial BBHs mergers are detected).

6.1.1 Astrophysical scenario

In this case, the progenitors of merging BBHs are formed at the end-point of stellar evolution. All the features of the detected GW events originated from their mergers are already discussed in section 3.1. GWs from mergers of astrophysical BHs will then highly correlate with large, luminous halos that contain the majority of stars, and, consequently, they would highly correlate with the HI IM signal. The average bias in the redshift range considered here (calculated combining equations (3.2) and (2.10)) is

$$\bar{b}_{\text{GW}}^{\text{ASTRO}} \sim 2.17. \quad (6.2)$$

Finally, by definition this scenario is characterized by a value of $\Gamma_{\text{pbh}} = 0$.

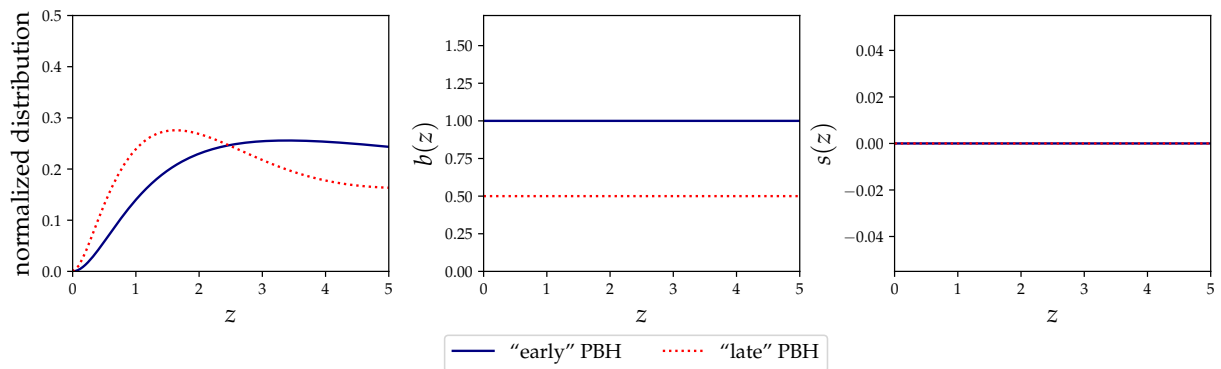


Figure 5. Specifics for the GW tracer in the “early” and “late” primordial scenarios. *Left:* normalized redshift distribution. *Center:* bias $b(z)$. *Right:* magnification bias $s(z)$. Magnification bias assumed to be zero for both scenarios (see appendix B for further discussions).

6.1.2 Primordial scenario: “early” binaries

We start our analysis of the GW \times IM that will be measured if $\Gamma_{\text{pbh}} \neq 0$ with the scenario in which the vast majority of primordial black holes binary formation took place in the early universe (see e.g., [184, 193]), while late time formed PBH binaries are assumed to give a negligible contribution.

In analogy to the correlation of GW with galaxies, the HI distribution is expected to correlate with PBHs mergers from early binaries with a different bias. This is due to the fact that these binaries would form in correspondence of the DM distribution, tracing very well the underlying matter distribution, instead of just tracing locations with massive and luminous halos. Assuming $\Gamma_{\text{pbh}} = 1.0$, GWs should have an associated bias of

$$\bar{b}_{\text{GW}}^{\text{PBH}} \sim 1.0 \quad (6.3)$$

since they would trace very effectively the underlying matter distribution. We provide in Figure 5 the specifics characterizing GWs events produced in this scenario. See appendix B for further explanations.

6.1.3 Primordial scenario: “late” binaries

Under this scenario we again assume that the progenitors of the merging BBHs have primordial origin, but the formation of the binary system itself takes place in the late Universe through a gravitational bremsstrahlung process [177].

We assume binary formation happens when two PBHs have a close encounter and their relative velocities are low enough that capture can take place and allows the binary formation. Given that the velocity dispersion is on average lower within small mass halos, which can not form large quantities of stars and are characterized by low values of the bias parameter, GWs in this case would be anti-correlated with luminous galaxies and (if $\Gamma_{\text{pbh}} = 1.0$) GWs would be expected to poorly trace luminous, highly star-forming massive halos and would be characterized by a bias value of

$$\bar{b}_{\text{GW}}^{\text{PBH}} \sim 0.5, \quad (6.4)$$

which is typical of the dark, low-mass halos in which this PBHs late binary formation effect would take place [177].

In Figure 5 we show the specifics characterizing GWs events under this scenario. See appendix B for further explanations.

6.1.4 Primordial scenario: “mixed” binaries

Finally, we consider a case in which we assume that the progenitors of the merging BBHs have primordial origin, with PBH binary formation taking place through both channels described by the “early” and “late” scenarios.

The bias parameter value of this model is given by the weighted average of the two values of equations (6.3) and (6.4). In particular, as an example case, we assume that around 70% of the PBHs mergers come from early binaries, whereas around the 30% is given by mergers of late binaries. This rough estimate comes from taking the lower and upper bounds of the LIGO/Virgo local merger rate estimates and associating them to the “late” and “early” scenarios respectively. In fact, even though according to part of the current literature the “early” scenario might be the dominant one, the issue is not settled yet. In this case we aim at taking into account both PBHs binary formation channels, considering a non-negligible contribution to the total PBHs merger rate from either mechanism. Assuming $\Gamma_{\text{pbh}} = 1.0$, this scenario is then characterized by:

$$\bar{b}_{\text{GW}}^{\text{PBH}} \sim 0.85. \quad (6.5)$$

6.2 Forecasts

We calculate the Signal-to-Noise ratio S/N to quantify how well a fiducial model (astrophysical or primordial) can be distinguished from an alternative one, by looking at the \bar{b}_{GW} value predicted by the two models:

$$\left(\frac{S}{N}\right)^2 = \frac{(\bar{b}_{\text{GW}}^{\text{Alternative}} - \bar{b}_{\text{GW}}^{\text{Fiducial}})^2}{\sigma_{\bar{b}_{\text{GW}}^{\text{Fiducial}}}^2}, \quad (6.6)$$

where $\sigma_{\bar{b}_{\text{GW}}^{\text{Fiducial}}}$ is the Fisher estimated error on \bar{b}_{GW} in the fiducial scenario. The biases values $\bar{b}_{\text{GW}}^{\text{Alternative}}$ and $\bar{b}_{\text{GW}}^{\text{Fiducial}}$ are those characterizing the models presented in section 6.1, depending on which of them is assumed as alternative or fiducial. We obtain $\sigma_{\bar{b}_{\text{GW}}^{\text{Fiducial}}}$ by making use of the same Fisher pipeline (parameters and fiducial values) of the analysis of section 5: $\{K^{\text{fg}}, \ln 10^{10} A_s, n_s, \omega_{\text{cdm}}, \omega_b, 100\theta_s, w_0, w_a, \bar{b}_{\text{GW}}, \bar{b}_{\text{HI}}\}$ for a total of 10 parameters. We set Planck priors on $\{\ln 10^{10} A_s, n_s, \omega_{\text{cdm}}, \omega_b, 100\theta_s\}$ [142].

We provide forecasts assuming the astrophysical model as fiducial, characterized by $\Gamma_{\text{pbh}}^{\text{FID}} = 0.0$. Regarding the alternative models to compare with, we consider a series of mixed astrophysical-primordial scenarios with $\Gamma_{\text{pbh}}^{\text{ALT}} \in [0.0, 1.0]$, with a bias given by

$$\bar{b}_{\text{GW}}^{\text{ALT}} = \bar{b}_{\text{GW}}^{\text{ASTRO}}(1 - \Gamma_{\text{pbh}}^{\text{ALT}}) + \bar{b}_{\text{GW}}^{\text{PBH}}\Gamma_{\text{pbh}}^{\text{ALT}}. \quad (6.7)$$

It is worth noting that this kind of approach may lead to possible degeneracies for some mixed scenarios, i.e., different scenarios combinations might yield the same \bar{b}_{GW} . In this eventuality, comparing the bias in specific redshift sub-samples would be enough to break the degeneracy, given that its predicted redshift dependence is different among distinct cases.

We provide in figure 6 SNR estimates from equation (6.6) for a series of values of f_{sky} and $T_{\text{obs}}^{\text{GW}}$ assuming the astrophysical scenario as fiducial and comparing it with the three different primordial scenarios (“early”, “late” and “mixed”) described in section 6.1. On the

left panel we show the SNR as a function of $\Gamma_{\text{pbh}}^{\text{ALT}}$, where the color code indicates the fraction of the sky observed. On the right panels we present the SNR obtainable (color coded) as a function of both the observation time and the fraction of primordial BBHs in the alternative model. In both columns, from top to bottom results for the three scenarios presented above are provided.

It can be seen that for large enough fractions of the sky and observation times, results are very promising, providing a S/N well above unity. In fact, it would be possible to distinguish, at a few sigma, a purely astrophysical model from an alternative model made up of similar relative abundances between astrophysical and primordial BBHs ($\Gamma_{\text{pbh}}^{\text{ALT}} \sim 0.5$) with a few years of observations and $f_{\text{sky}} \sim 0.5$. In addition, an alternative model with low values of $\Gamma_{\text{pbh}}^{\text{ALT}}$ (i.e., mostly made of astrophysical BHs) such as $\Gamma_{\text{pbh}}^{\text{ALT}} \sim 0.2$, could be detected within 10 years of observation for $f_{\text{sky}} = 0.5$, that we stress once again being the fiducial value for the considered SKAO-MID survey. We have also tested mixed scenarios with different relative abundances of early/late-type PBHs to astrophysical BHs, finding as expected no extremely different qualitative behaviours when changing these quantities.

Finally, analogous conclusions can be reached when the assumed fiducial model is a primordial scenario: for completeness, we provide forecasts for the example case of “early” primordial scenario assumed as fiducial in appendix B.

7 Conclusions

In this work, we investigated the cross-correlation signal between gravitational wave catalogs and HI intensity maps that could be potentially measured with future experiments such as the Einstein Telescope and the SKA Observatory. We extended the range of applications of the publicly available code `Multi_CLASS`, by including signal from the IM unresolved HI sources and compute their angular power spectra C_ℓ s, including all projection effects over a variety of redshift ranges.

We presented three cosmological and astrophysical applications we believe will be particularly exciting for the future.

First, we investigated how well the $\text{GW} \times \text{IM}$ cross-correlation can provide model independent and agnostic information on the redshift distribution of resolved binary black hole mergers. Our results show that we will be able to obtain good precision in the inferred statistical redshift distribution of BBH merger number counts. With the experiments considered, we will be able to obtain a precision of order a few tens of % for redshifts up to $z \approx 1.5$, potentially providing ways to discriminate between different astrophysical models of the binary formation, evolution and mergers.

We stress that our methodology does not make use of any astrophysical model, including BH population, mass function, etc, and is free from assumptions on the values of the cosmological parameters. It will be of particular interest to compare results from our methodology with other approaches that either assume the knowledge of a cosmological model, set priors on the BH population distributions or exploit machine learning techniques (see e.g., [48, 50, 143]). The combinations of these methods could lead to an improvement of constraints or, if some inconsistencies will emerge, could provide hints of inaccuracies in standard assumptions.

Measurements of power spectra of tracers of the matter distribution over cosmic epochs will naturally provide also cosmological information; as an example showcasing the potential of the $\text{GW} \times \text{IM}$ observable, we forecast constraints on dynamical dark energy parameters. Our results show that the $\text{GW} \times \text{IM}$ cross-correlations will provide a fundamental validation

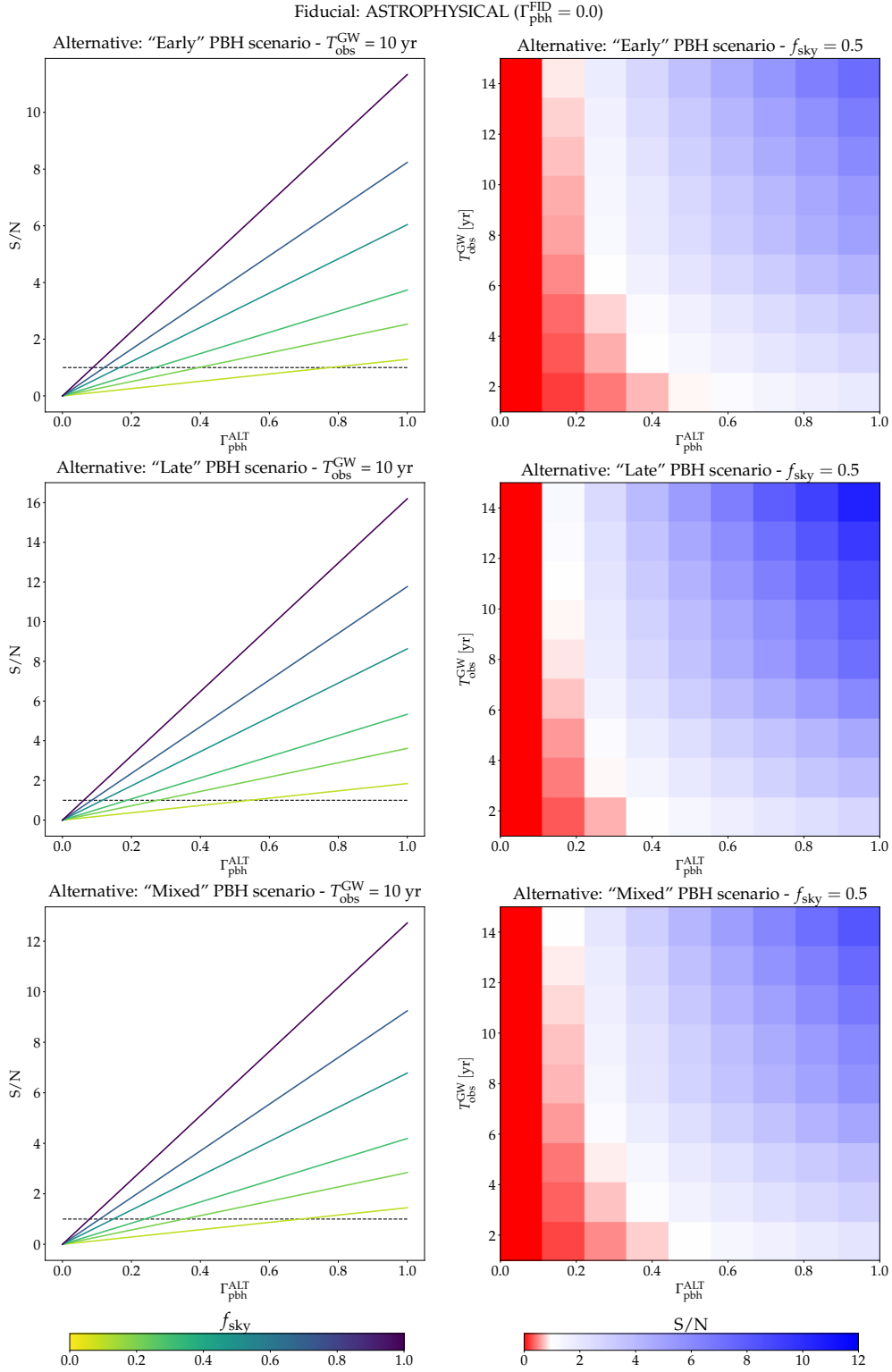


Figure 6. SNR for different values of $T_{\text{obs}}^{\text{GW}}$ (from 1 yr to 15 yr), f_{sky} (from 0.1 to 1.0) and $\Gamma_{\text{pbh}}^{\text{ALT}}$ (from 0.0 to 1.0), assuming the astrophysical model as fiducial. The alternative model assumed is the “Early”, “Late” and “Mixed” primordial scenario in the top, center and bottom panel, respectively. The colorbar of the right-side plots is normalized to white at $S/N = 1$.

of IM-only results, as this latter could be a measurement affected by unknown systematic errors.

As a final application for $\text{GW} \times \text{IM}$, we studied how we can use this correlation to detect a primordial component in the BBHs detected through GW from their mergers. We follow the approach of [38, 39] and extend it to HI IM maps, at the same time updating merger rate estimates and binary formation channels with the latest results available in literature. Compared to the case of the correlation with star forming galaxies, using IM allows us to reach higher redshifts and have a very fine tomographic binning. Our results show that with $\text{GW} \times \text{IM}$ from the ET and SKAO we will be able to detect the presence of a PBH component down to about 30% of detected mergers at high Signal-to-Noise ratios.

To conclude, we presented the first study of the cross-correlation between gravitational waves from resolved binary black hole mergers and the HI intensity mapping signal, and investigated some possible interesting applications with predictions from the future Einstein Telescope and SKAO experiments. We believe that this first investigation can open up a plethora of new measurements and possibilities for the scientific community. Moreover, it will be of particular interest to combine our suggested approach with other ones such as additional $\text{GW} \times \text{LSS}$ correlations. This paper can be seen as part of the ongoing effort to develop multi-tracer approaches, which has an enormous potential in both cosmology and astrophysics, as it allows to test models in ways that would not be possible by looking at single tracers separately.

Acknowledgments

We are thankful to José Luis Bernal, Kaze Wong and Gabriela Sato-Polito for their helpful advices. We thank Nicola Bellomo, Alessandro Bressan, Phil Bull, Stefano Camera, Jose Fonseca, Ely Kovetz, Suvodip Mukherjee, Julian Muñoz, Gabriele Parimbelli, Mario Spera for useful discussions. GS, MS and MV are supported by the INFN PD51 INDARK grant. MS acknowledges funding from the INAF PRIN-SKA 2017 project 1.05.01.88.04 (FORECaST). AR acknowledges funding from Italian Ministry of University and Research (MIUR) through the “Dipartimenti di eccellenza” project “Science of the Universe”. AL acknowledges funding from PRIN MIUR 2017 prot. 20173ML3WW, ‘Opening the ALMA window on the cosmic evolution of gas, stars and supermassive black holes’, and from the EU H2020-MSCA-ITN-2019 Project 860744 ‘BiD4BESt: Big Data applications for black hole Evolution STudies’.

A Relativistic number counts

In this appendix we provide the complete expressions for the relativistic number counts effects introduced in equation (2.9):

$$\begin{aligned}
\Delta_\ell^{\text{den}}(k, z) &= b_X \delta(k, \tau_z) j_\ell, \\
\Delta_\ell^{\text{vel}}(k, z) &= \frac{k}{\mathcal{H}} j_\ell'' V(k, \tau_z) + \left[(f_X^{\text{evo}} - 3) \frac{\mathcal{H}}{k} j_\ell + \left(\frac{\mathcal{H}'}{\mathcal{H}^2} + \frac{2 - 5s_X}{r(z)\mathcal{H}} + 5s_X - f_X^{\text{evo}} \right) j_\ell' \right] V(k, \tau_z), \\
\Delta_\ell^{\text{len}}(k, z) &= \ell(\ell + 1) \frac{2 - 5s_X}{2} \int_0^{r(z)} dr \frac{r(z) - r}{r(z)r} [\Phi(k, \tau_z) + \Psi(k, \tau_z)] j_\ell(kr), \\
\Delta_\ell^{\text{gr}}(k, z) &= \left[\left(\frac{\mathcal{H}'}{\mathcal{H}^2} + \frac{2 - 5s_X}{r(z)\mathcal{H}} + 5s_X - f_X^{\text{evo}} + 1 \right) \Psi(k, \tau_z) + (-2 + 5s_X) \Phi(k, \tau_z) + \mathcal{H}^{-1} \Phi'(k, \tau_z) \right] j_\ell + \\
&\quad + \int_0^{r(z)} dr \frac{2 - 5s_X}{r(z)} [\Phi(k, \tau) + \Psi(k, \tau)] j_\ell(kr) \\
&\quad + \int_0^{r(z)} dr \left(\frac{\mathcal{H}'}{\mathcal{H}^2} + \frac{2 - 5s_X}{r(z)\mathcal{H}} + 5s_X - f_X^{\text{evo}} \right)_{r(z)} [\Phi'(k, \tau) + \Psi'(k, \tau)] j_\ell(kr).
\end{aligned} \tag{A.1}$$

The quantities introduced above have the following physical meaning: b_X is the bias parameter, s_X is the magnification bias parameter, f_X^{evo} is the evolution bias parameter, r is the conformal distance on the light cone, $\tau = \tau_0 - r$ is the conformal time, $\tau_z = \tau_0 - r(z)$, j_ℓ , $j_\ell' = \frac{dj_\ell}{dy}$, $j_\ell'' = \frac{d^2j_\ell}{dy^2}$ are the Bessel functions and their derivatives (evaluated at $y = kr(z)$ when not explicitly stated), \mathcal{H} is the conformal Hubble parameter, the prime symbol ' indicates derivatives with respect to conformal time, δ is the density contrast in the comoving gauge, V is the peculiar velocity, Φ and Ψ are Bardeen potentials (see e.g., reference [89] and references therein).

B Astrophysical vs. primordial BBHs: “early” primordial scenario as fiducial

For completeness, in this appendix we show that the optimistic results of section 6, regarding the possibility of determining the progenitors of merging BBHs, are obtainable also when considering a primordial scenario as fiducial model, aiming at distinguishing it from an alternative astrophysical case.

We consider here the “early” primordial scenario and assume the redshift evolution of the merger rate described in reference [193], which is an extension to the model of reference [184]. As done for the astrophysical merger rate, we re-normalize it to the value of $30 \text{ Gpc}^{-3} \text{ yr}^{-1}$, in agreement with local LIGO/Virgo observations. In fact, suppression effects to the merger rate could in principle shift it to agree with experimental values [193]. We stress that due to the big uncertainties of both the PBHs merger rate and suppression effects, the state of the art in this field is still in full development.

Given the big uncertainties in the PBH modeling, we assume here a magnification bias with a value of $s_{\text{GW}}^{\text{PBH}} = 0.0$, since almost all sources in the $\mathcal{O}(10M_\odot)$ mass range would be detected by the ET in our redshift interval (see e.g., figure 3 of [39]) and a slightly more precise determination of this quantity would be possible only by fixing quantities accompanied by huge uncertainties (mass distribution, suppression model, etc.). We provide in figure 5 the

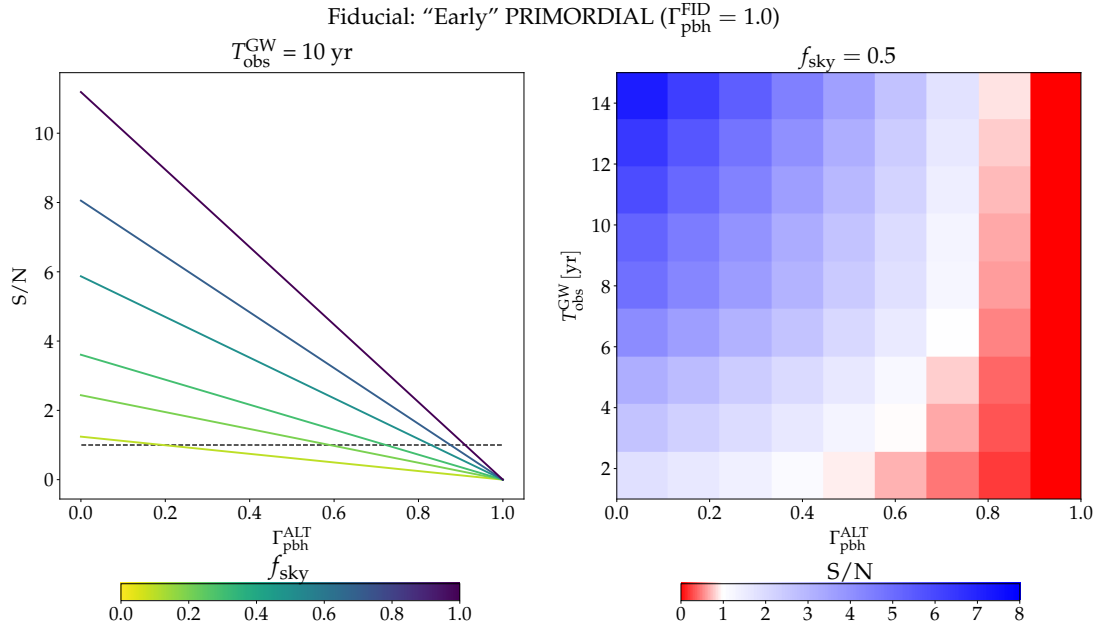


Figure 7. S/N ratios for distinguishing the Fiducial scenario from the Alternative, for different values of $T_{\text{obs}}^{\text{GW}}$ (from 1 yr to 15 yr), f_{sky} (from 0.1 to 1.0) and $\Gamma_{\text{pbh}}^{\text{ALT}}$ (from 0.0 to 1.0). “Early” primordial model assumed as Fiducial. Models with different $\Gamma_{\text{pbh}}^{\text{ALT}}$ assumed as Alternative. The colorbar of the right-side plots is normalized to white at $S/N = 1$.

specifics assumed for this scenario, comparing them for completeness with those of the “late” primordial case (redshift distribution following prescriptions of reference [177]).

As figure 7 shows, high values of the SNR would be reached even for relatively low values of f_{sky} and $T_{\text{obs}}^{\text{GW}}$, in analogy with results from figure 6, in which the astrophysical scenario is instead assumed as fiducial.

References

- [1] The **LIGO Scientific Collaboration and Virgo Collaboration**, B. P. Abbott *et al.*, “Observation of Gravitational Waves from a Binary Black Hole Merger”, [*Phys. Rev. Lett.* **116** \(Feb, 2016\) 061102](#), [arXiv:1602.03837](#).
- [2] The **LIGO Scientific Collaboration and Virgo Collaboration**, B. P. Abbott *et al.*, “Properties of the Binary Black Hole Merger GW150914”, [*Phys. Rev. Lett.* **116** \(Jun, 2016\) 241102](#), [arXiv:1602.03840](#).
- [3] The **LIGO Scientific Collaboration and Virgo Collaboration**, B. P. Abbott *et al.*, “GWTC-1: A Gravitational-Wave Transient Catalog of Compact Binary Mergers Observed by LIGO and Virgo during the First and Second Observing Runs”, [*Phys. Rev. X* **9** \(Sep, 2019\) 031040](#).
- [4] The **LIGO Scientific Collaboration and Virgo Collaboration**, R. Abbott *et al.*, “GWTC-2: Compact Binary Coalescences Observed by LIGO and Virgo during the First Half of the Third Observing Run”, [*Phys. Rev. X* **11** \(Jun, 2021\) 021053](#).
- [5] E. D. Kovetz, M. P. Viero, A. Lidz, L. Newburgh, M. Rahman, E. Switzer, M. Kamionkowski, J. Aguirre, M. Alvarez, J. Bock, *et al.*, “Line-intensity mapping: 2017 status report”, [arXiv preprint arXiv:1709.09066](#) (2017) .

- [6] T.-C. Chang, U.-L. Pen, K. Bandura, and J. B. Peterson, “An intensity map of hydrogen 21-cm emission at redshift $z \sim 0.8$ ”, [Nature](#) **466** no. 7305, (July, 2010) 463–465.
- [7] K. W. Masui, E. R. Switzer, N. Banavar, K. Bandura, C. Blake, L. M. Calin, T. C. Chang, X. Chen, Y. C. Li, Y. W. Liao, A. Natarajan, U. L. Pen, J. B. Peterson, J. R. Shaw, and T. C. Voytek, “Measurement of 21 cm Brightness Fluctuations at $z \sim 0.8$ in Cross-correlation”, [The Astrophysical Journal Letters](#) **763** no. 1, (Jan., 2013) L20, [arXiv:1208.0331 \[astro-ph.CO\]](#).
- [8] C. J. Anderson, N. J. Luciw, Y. C. Li, C. Y. Kuo, J. Yadav, K. W. Masui, T. C. Chang, X. Chen, N. Oppermann, Y. W. Liao, U. L. Pen, D. C. Price, L. Staveley-Smith, E. R. Switzer, P. T. Timbie, and L. Wolz, “Low-amplitude clustering in low-redshift 21-cm intensity maps cross-correlated with 2dF galaxy densities”, [Monthly Notices of the Royal Astronomical Society](#) **476** no. 3, (May, 2018) 3382–3392, [arXiv:1710.00424 \[astro-ph.CO\]](#).
- [9] L. Wolz, A. Pourtsidou, K. W. Masui, T.-C. Chang, J. E. Bautista, E.-M. Müller, S. Avila, D. Bacon, W. J. Percival, S. Cunnington, et al., “HI constraints from the cross-correlation of eBOSS galaxies and Green Bank Telescope intensity maps”, [arXiv preprint arXiv:2102.04946](#) (2021) .
- [10] F. Villaescusa-Navarro, M. Viel, K. K. Datta, and T. R. Choudhury, “Modeling the neutral hydrogen distribution in the post-reionization Universe: intensity mapping”, [Journal of Cosmology and Astroparticle Physics](#) **2014** no. 09, (2014) 050.
- [11] R. Braun, T. L. Bourke, J. A. Green, E. Keane, and J. Wagg, “Advancing astrophysics with the square kilometre array”, in *Advancing Astrophysics with the Square Kilometre Array*, vol. 215, p. 174, SISSA Medialab. 2015.
- [12] M. G. Santos, M. Cluver, M. Hilton, M. Jarvis, G. I. Jozsa, L. Leeuw, O. Smirnov, R. Taylor, F. Abdalla, J. Afonso, et al., “MeerKLASS: MeerKAT large area synoptic survey”, [arXiv preprint arXiv:1709.06099](#) (2017) .
- [13] J. Wang, M. G. Santos, P. Bull, K. Grainge, S. Cunnington, J. Fonseca, M. O. Irfan, Y. Li, A. Pourtsidou, P. S. Soares, et al., “HI intensity mapping with MeerKAT: Calibration pipeline for multi-dish autocorrelation observations”, [arXiv preprint arXiv:2011.13789](#) (2020) .
- [14] D. J. Bacon, R. A. Battye, P. Bull, S. Camera, P. G. Ferreira, I. Harrison, D. Parkinson, A. Pourtsidou, M. G. Santos, L. Wolz, and et al., “Cosmology with Phase 1 of the Square Kilometre Array Red Book 2018: Technical specifications and performance forecasts”, [Publications of the Astronomical Society of Australia](#) **37** (2020) e007.
- [15] R. Maartens, F. B. Abdalla, M. Jarvis, and M. G. Santos, “Cosmology with the SKA – overview”, 2015.
- [16] M. G. Santos, P. Bull, D. Alonso, S. Camera, P. G. Ferreira, G. Bernardi, R. Maartens, M. Viel, F. Villaescusa-Navarro, F. B. Abdalla, et al., “Cosmology with a SKA HI intensity mapping survey”, [arXiv preprint arXiv:1501.03989](#) (2015) .
- [17] K. Bandura et al., “Canadian Hydrogen Intensity Mapping Experiment (CHIME) pathfinder”, in *Ground-based and Airborne Telescopes V*, L. M. Stepp, R. Gilmozzi, and H. J. Hall, eds., vol. 9145 of *Society of Photo-Optical Instrumentation Engineers (SPIE) Conference Series*, p. 914522. July, 2014. [arXiv:1406.2288 \[astro-ph.IM\]](#).
- [18] W. Hu, X. Wang, F. Wu, Y. Wang, P. Zhang, and X. Chen, “Forecast for FAST: from galaxies survey to intensity mapping”, [Monthly Notices of the Royal Astronomical Society](#) **493** no. 4, (Apr., 2020) 5854–5870, [arXiv:1909.10946 \[astro-ph.CO\]](#).
- [19] R. Battye et al., “Update on the BINGO 21cm intensity mapping experiment”, [arXiv e-prints](#) (Oct., 2016) [arXiv:1610.06826](#), [arXiv:1610.06826 \[astro-ph.CO\]](#).
- [20] S. Das et al., “Progress in the construction and testing of the Tianlai radio interferometers”, in *Millimeter, Submillimeter, and Far-Infrared Detectors and Instrumentation for Astronomy IX*,

- J. Zmuidzinas and J.-R. Gao, eds., vol. 10708 of *Society of Photo-Optical Instrumentation Engineers (SPIE) Conference Series*, p. 1070836. July, 2018. [arXiv:1806.04698](#) [[astro-ph.IM](#)].
- [21] L. B. Newburgh et al., “[HIRAX: a probe of dark energy and radio transients](#)”, in *Ground-based and Airborne Telescopes VI*, H. J. Hall, R. Gilmozzi, and H. K. Marshall, eds., vol. 9906 of *Society of Photo-Optical Instrumentation Engineers (SPIE) Conference Series*, p. 99065X. Aug., 2016. [arXiv:1607.02059](#) [[astro-ph.IM](#)].
- [22] M. R. Nolta, E. Wright, L. Page, C. Bennett, M. Halpern, G. Hinshaw, N. Jarosik, A. Kogut, M. Limon, S. Meyer, et al., “First year Wilkinson microwave anisotropy probe observations: dark energy induced correlation with radio sources”, *The Astrophysical Journal* **608** no. 1, (2004) 10.
- [23] S. Ho, C. Hirata, N. Padmanabhan, U. Seljak, and N. Bahcall, “Correlation of CMB with large-scale structure. I. Integrated Sachs-Wolfe tomography and cosmological implications”, *Physical Review D* **78** no. 4, (2008) 043519.
- [24] C. M. Hirata, S. Ho, N. Padmanabhan, U. Seljak, and N. A. Bahcall, “Correlation of CMB with large-scale structure. II. Weak lensing”, *Physical Review D* **78** no. 4, (2008) 043520.
- [25] A. Raccanelli, A. Bonaldi, M. Negrello, S. Matarrese, G. Tormen, and G. De Zotti, “A reassessment of the evidence of the Integrated Sachs-Wolfe effect through the WMAP-NVSS correlation”, *Monthly Notices of the Royal Astronomical Society* **386** no. 4, (2008) 2161–2166, [arXiv:0802.0084](#).
- [26] A. Raccanelli, G.-B. Zhao, D. J. Bacon, M. J. Jarvis, W. J. Percival, R. P. Norris, H. Röttgering, F. B. Abdalla, C. M. Cress, J.-C. Kubwimana, S. Lindsay, R. C. Nichol, M. G. Santos, and D. J. Schwarz, “Cosmological measurements with forthcoming radio continuum surveys”, *Monthly Notices of the Royal Astronomical Society* **424** no. 2, (Aug., 2012) 801–819, [arXiv:1108.0930](#) [[astro-ph.CO](#)].
- [27] A. Raccanelli, O. Doré, D. J. Bacon, R. Maartens, M. G. Santos, S. Camera, T. M. Davis, M. J. Drinkwater, M. Jarvis, R. Norris, and D. Parkinson, “Probing primordial non-Gaussianity via iSW measurements with SKA continuum surveys”, *Journal of Cosmology and Astroparticle Physics* **2015** no. 1, (Jan., 2015) 042, [arXiv:1406.0010](#) [[astro-ph.CO](#)].
- [28] The **Herschel ATLAS**, F. Bianchini et al., “Cross-correlation between the CMB lensing potential measured by Planck and high-z sub-mm galaxies detected by the Herschel-ATLAS survey”, *Astrophys. J.* **802** no. 1, (2015) 64, [arXiv:1410.4502](#) [[astro-ph.CO](#)].
- [29] F. Bianchini and A. Lapi, “Cross-correlation between cosmological and astrophysical datasets: the Planck and Herschel case”, *IAU Symp.* **306** (2014) 202–205.
- [30] F. Bianchini et al., “Toward a tomographic analysis of the cross-correlation between Planck CMB lensing and H-ATLAS galaxies”, *Astrophys. J.* **825** no. 1, (2016) 24, [arXiv:1511.05116](#) [[astro-ph.CO](#)].
- [31] S. Mukherjee, B. D. Wandelt, and J. Silk, “Multimessenger tests of gravity with weakly lensed gravitational waves”, *Phys. Rev. D* **101** (May, 2020) 103509.
- [32] K. Fang, A. Banerjee, E. Charles, and Y. Omori, “A Cross-Correlation Study of High-energy Neutrinos and Tracers of Large-Scale Structure”, *The Astrophysical Journal* **894** no. 2, (2020) 112.
- [33] H. J. Martínez, M. E. Merchán, C. A. Valotto, and D. G. Lambas, “Quasar-galaxy and AGN-galaxy cross-correlations”, *The Astrophysical Journal* **514** no. 2, (1999) 558.
- [34] B. Jain, R. Scranton, and R. K. Sheth, “Quasar—galaxy and galaxy—galaxy cross-correlations: model predictions with realistic galaxies”, *Monthly Notices of the Royal Astronomical Society* **345** no. 1, (10, 2003) 62–70.

- [35] X. Yang, H. J. Mo, F. C. van den Bosch, S. M. Weinmann, C. Li, and Y. P. Jing, “The cross-correlation between galaxies and groups: probing the galaxy distribution in and around dark matter haloes”, [*Monthly Notices of the Royal Astronomical Society* **362** no. 2, \(09, 2005\) 711–726](#).
- [36] K. Paech, N. Hamaus, B. Hoyle, M. Costanzi, T. Giannantonio, S. Hagstotz, G. Sauerwein, and J. Weller, “Cross-correlation of galaxies and galaxy clusters in the Sloan Digital Sky Survey and the importance of non-Poissonian shot noise”, [*Monthly Notices of the Royal Astronomical Society* **470** no. 3, \(06, 2017\) 2566–2577](#).
- [37] M. Oguri, “Measuring the distance-redshift relation with the cross-correlation of gravitational wave standard sirens and galaxies”, [*Physical Review D* **93** no. 8, \(Apr., 2016\) 083511](#), [arXiv:1603.02356 \[astro-ph.CO\]](#).
- [38] A. Raccanelli, E. D. Kovetz, S. Bird, I. Cholis, and J. B. Muñoz, “Determining the progenitors of merging black-hole binaries”, [*Phys. Rev. D* **94** \(Jul, 2016\) 023516](#), [arXiv:1605.01405](#).
- [39] G. Scelfo, N. Bellomo, A. Raccanelli, S. Matarrese, and L. Verde, “GW×LSS: chasing the progenitors of merging binary black holes”, [*JCAP* **2018** no. 09, \(Sep, 2018\) 039–039](#), [arXiv:1809.03528v1](#).
- [40] G. Scelfo, L. Boco, A. Lapi, and M. Viel, “Exploring galaxies-gravitational waves cross-correlations as an astrophysical probe”, [*Journal of Cosmology and Astroparticle Physics* **2020** no. 10, \(Oct, 2020\) 045–045](#).
- [41] T. Namikawa, A. Nishizawa, and A. Taruya, “Anisotropies of gravitational-wave standard sirens as a new cosmological probe without redshift information”, [*Physical review letters* **116** no. 12, \(2016\) 121302](#).
- [42] D. Alonso, G. Cusin, P. G. Ferreira, and C. Pitrou, “Detecting the anisotropic astrophysical gravitational wave background in the presence of shot noise through cross-correlations”, [arXiv:2002.02888](#).
- [43] G. Cañas Herrera, O. Contigiani, and V. Vardanyan, “Cross-correlation of the astrophysical gravitational-wave background with galaxy clustering”, [*Phys. Rev. D* **102** \(Aug, 2020\) 043513](#).
- [44] F. Calore, A. Cuoco, T. Regimbau, S. Sachdev, and P. D. Serpico, “Cross-correlating galaxy catalogs and gravitational waves: a tomographic approach”, [*Physical Review Research* **2** no. 2, \(2020\) 023314](#).
- [45] S. Camera and A. Nishizawa, “Beyond Concordance Cosmology with Magnification of Gravitational-Wave Standard Sirens”, [*Phys. Rev. Lett.* **110** \(Apr, 2013\) 151103](#), [arXiv:1303.5446](#).
- [46] S. Libanore, M. C. Artale, D. Karagiannis, M. Liguori, N. Bartolo, Y. Bouffanais, N. Giacobbo, M. Mapelli, and S. Matarrese, “Gravitational Wave mergers as tracers of Large Scale Structures”, [*Journal of Cosmology and Astroparticle Physics* **2021** no. 02, \(Feb, 2021\) 035–035](#). <https://doi.org/10.1088/1475-7516/2021/02/035>.
- [47] S. Mukherjee, B. D. Wandelt, and J. Silk, “Probing the theory of gravity with gravitational lensing of gravitational waves and galaxy surveys”, [*Monthly Notices of the Royal Astronomical Society* **494** no. 2, \(03, 2020\) 1956–1970](#).
- [48] S. Mukherjee, B. D. Wandelt, S. M. Nissanke, and A. Silvestri, “Accurate precision cosmology with redshift unknown gravitational wave sources”, [*Phys. Rev. D* **103** \(Feb, 2021\) 043520](#).
- [49] S. Mukherjee and J. Silk, “Time dependence of the astrophysical stochastic gravitational wave background”, [*Monthly Notices of the Royal Astronomical Society* **491** no. 4, \(11, 2019\) 4690–4701](#).
- [50] G. Cañas-Herrera, O. Contigiani, and V. Vardanyan, “Learning how to surf: Reconstructing

the propagation and origin of gravitational waves with Gaussian Processes”, [arXiv preprint arXiv:2105.04262](#) (2021) .

- [51] S. J. Schmidt, B. Ménard, R. Scranton, C. Morrison, and C. K. McBride, “Recovering redshift distributions with cross-correlations: pushing the boundaries”, [Monthly Notices of the Royal Astronomical Society](#) **431** no. 4, (04, 2013) 3307–3318.
- [52] D. Alonso and P. G. Ferreira, “Constraining ultralarge-scale cosmology with multiple tracers in optical and radio surveys”, [Phys. Rev. D](#) **92** (Sep, 2015) 063525.
- [53] E. D. Kovetz, A. Raccanelli, and M. Rahman, “Cosmological constraints with clustering-based redshifts”, [Monthly Notices of the Royal Astronomical Society](#) **468** no. 3, (03, 2017) 3650–3656.
- [54] D. Alonso and P. G. Ferreira, “Constraining ultralarge-scale cosmology with multiple tracers in optical and radio surveys”, [Phys. Rev. D](#) **92** (Sep, 2015) 063525.
- [55] L. Wolz, C. Tonini, C. Blake, and J. S. B. Wyithe, “Intensity mapping cross-correlations: connecting the largest scales to galaxy evolution”, [Monthly Notices of the Royal Astronomical Society](#) **458** no. 3, (03, 2016) 3399–3410.
- [56] A. Pourtsidou, D. Bacon, R. Crittenden, and R. B. Metcalf, “Prospects for clustering and lensing measurements with forthcoming intensity mapping and optical surveys”, [Monthly Notices of the Royal Astronomical Society](#) **459** no. 1, (03, 2016) 863–870.
- [57] A. Pourtsidou, “Testing gravity at large scales with HI intensity mapping”, [Monthly Notices of the Royal Astronomical Society](#) **461** no. 2, (06, 2016) 1457–1464.
- [58] A. Raccanelli, E. Kovetz, L. Dai, and M. Kamionkowski, “Detecting the integrated Sachs-Wolfe effect with high-redshift 21-cm surveys”, [Phys. Rev. D](#) **93** (Apr, 2016) 083512. <https://link.aps.org/doi/10.1103/PhysRevD.93.083512>.
- [59] A. Pourtsidou, D. Bacon, and R. Crittenden, “HI and cosmological constraints from intensity mapping, optical and CMB surveys”, [Monthly Notices of the Royal Astronomical Society](#) **470** no. 4, (06, 2017) 4251–4260.
- [60] L. Wolz, C. Blake, and J. S. B. Wyithe, “Determining the HI content of galaxies via intensity mapping cross-correlations”, [Monthly Notices of the Royal Astronomical Society](#) **470** no. 3, (06, 2017) 3220–3226.
- [61] D. Alonso, P. G. Ferreira, M. J. Jarvis, and K. Moodley, “Calibrating photometric redshifts with intensity mapping observations”, [Phys. Rev. D](#) **96** (Aug, 2017) 043515.
- [62] L. Wolz, S. G. Murray, C. Blake, and J. S. Wyithe, “Intensity mapping cross-correlations II: HI halo models including shot noise”, [Monthly Notices of the Royal Astronomical Society](#) **484** no. 1, (11, 2018) 1007–1020.
- [63] S. Cunnington, I. Harrison, A. Pourtsidou, and D. Bacon, “HI intensity mapping for clustering-based redshift estimation”, [Monthly Notices of the Royal Astronomical Society](#) **482** no. 3, (10, 2018) 3341–3355.
- [64] B. Sathyaprakash et al., “Scientific objectives of Einstein Telescope”, [Classical and Quantum Gravity](#) **29** no. 12, (2012) 124013, [arXiv:1206.0331](#).
- [65] J. A. Newman, “Calibrating Redshift Distributions beyond Spectroscopic Limits with Cross-Correlations”, [The Astrophysical Journal](#) **684** no. 1, (Sep, 2008) 88–101.
- [66] J. Benjamin, L. Van Waerbeke, B. Ménard, and M. Kilbinger, “Photometric redshifts: estimating their contamination and distribution using clustering information”, [Monthly Notices of the Royal Astronomical Society](#) **408** no. 2, (10, 2010) 1168–1180.
- [67] D. J. Matthews and J. A. Newman, “Reconstructing Redshift Distributions with

- Cross-Correlations: Tests and an Optimized Recipe”, [The Astrophysical Journal](#) **721** no. 1, (Aug, 2010) 456–468.
- [68] S. J. Schmidt, B. Ménard, R. Scranton, C. Morrison, and C. K. McBride, “Recovering redshift distributions with cross-correlations: pushing the boundaries”, [Monthly Notices of the Royal Astronomical Society](#) **431** no. 4, (04, 2013) 3307–3318.
- [69] B. Ménard, R. Scranton, S. Schmidt, C. Morrison, D. Jeong, T. Budavari, and M. Rahman, “Clustering-based redshift estimation: method and application to data”, [arXiv preprint arXiv:1303.4722](#) (2013) .
- [70] M. McQuinn and M. White, “On using angular cross-correlations to determine source redshift distributions”, [Monthly Notices of the Royal Astronomical Society](#) **433** no. 4, (07, 2013) 2857–2883.
- [71] A. Choi, C. Heymans, C. Blake, H. Hildebrandt, C. A. J. Duncan, T. Erben, R. Nakajima, L. Van Waerbeke, and M. Viola, “CFHTLenS and RCSLenS: testing photometric redshift distributions using angular cross-correlations with spectroscopic galaxy surveys”, [Monthly Notices of the Royal Astronomical Society](#) **463** no. 4, (09, 2016) 3737–3754.
- [72] V. Scottetz, Y. Mellier, B. R. Granett, Moutard, *et al.*, “Clustering-based redshift estimation: application to VIPERS/CFHTLS”, [Monthly Notices of the Royal Astronomical Society](#) **462** no. 2, (07, 2016) 1683–1696.
- [73] M. Rahman, B. Ménard, and R. Scranton, “Exploring the 2MASS extended and point source catalogues with clustering redshifts”, [Monthly Notices of the Royal Astronomical Society](#) **457** no. 4, (02, 2016) 3912–3921.
- [74] A. Johnson, C. Blake, A. Amon, T. Erben, *et al.*, “2dFLenS and KiDS: determining source redshift distributions with cross-correlations”, [Monthly Notices of the Royal Astronomical Society](#) **465** no. 4, (11, 2016) 4118–4132.
- [75] M. P. van Daalen and M. White, “A cross-correlation-based estimate of the galaxy luminosity function”, [Monthly Notices of the Royal Astronomical Society](#) **476** no. 4, (03, 2018) 4649–4661.
- [76] D. Alonso, E. Bellini, C. Hale, M. J. Jarvis, and D. J. Schwarz, “Cross-correlating radio continuum surveys and CMB lensing: constraining redshift distributions, galaxy bias, and cosmology”, [Monthly Notices of the Royal Astronomical Society](#) **502** no. 1, (01, 2021) 876–887.
- [77] P. Peebles, “Statistical analysis of catalogs of extragalactic objects. I. Theory”, [The Astrophysical Journal](#) **185** (1973) 413–440.
- [78] P. PEEBLES, “The large-scale structure of the universe(Book)”, [Research supported by the National Science Foundation. Princeton, N. J., Princeton University Press, 1980. 435 p](#) (1980) .
- [79] E. Regos and A. S. Szalay, “Multipole expansion of the large-scale velocity field-Using the tensor window function”, [The Astrophysical Journal](#) **345** (1989) 627–636.
- [80] C. Scharf, Y. Hoffman, O. Lahav, and D. Lynden-Bell, “Spherical harmonic analysis of IRAS galaxies: implications for the Great Attractor and Cold Dark Matter”, [Monthly Notices of the Royal Astronomical Society](#) **256** no. 2, (05, 1992) 229–237.
- [81] O. Lahav, K. Fisher, Y. Hoffman, C. Scharf, and S. Zaroubi, “Wiener reconstruction of galaxy surveys in spherical harmonics”, [arXiv preprint astro-ph/9311059](#) (1993) .
- [82] K. B. Fisher, C. A. Scharf, and O. Lahav, “A spherical harmonic approach to redshift distortion and a measurement of Ω_0 from the 1.2-Jy IRAS Redshift Survey”, [Monthly Notices of the Royal Astronomical Society](#) **266** no. 1, (01, 1994) 219–226.
- [83] H. S. G. Gebhardt and D. Jeong, “Fast and accurate computation of projected two-point functions”, [Physical Review D](#) **97** no. 2, (2018) 023504.

- [84] V. Assassi, M. Simonović, and M. Zaldarriaga, “Efficient evaluation of angular power spectra and bispectra”, [Journal of Cosmology and Astroparticle Physics](#) **2017** no. 11, (2017) 054.
- [85] A. Raccanelli and Z. Vlah, “Unequal-time effects in the LSS correlators”, [in preparation](#) (2022) .
- [86] A. Challinor and A. Lewis, “Linear power spectrum of observed source number counts”, [Phys. Rev. D](#) **84** (Aug, 2011) 043516, [arXiv:1105.5292](#).
- [87] C. Bonvin and R. Durrer, “What galaxy surveys really measure”, [Phys. Rev. D](#) **84** (Sep, 2011) 063505, [arXiv:1105.5280](#).
- [88] D. Blas, J. Lesgourgues, and T. Tram, “The Cosmic Linear Anisotropy Solving System (CLASS). Part II: Approximation schemes”, [Journal of Cosmology and Astroparticle Physics](#) **2011** no. 07, (2011) 034, [arXiv:1104.2933](#).
- [89] E. D. Dio, F. Montanari, J. Lesgourgues, and R. Durrer, “The CLASSgal code for relativistic cosmological large scale structure”, [Journal of Cosmology and Astroparticle Physics](#) **2013** no. 11, (2013) 044, [arXiv:1307.1459](#).
- [90] N. Bellomo, J. L. Bernal, G. Scelfo, A. Raccanelli, and L. Verde, “Beware of commonly used approximations. Part I. Errors in forecasts”, [Journal of Cosmology and Astroparticle Physics](#) **2020** no. 10, (Oct, 2020) 016–016.
- [91] J. L. Bernal, N. Bellomo, A. Raccanelli, and L. Verde, “Beware of commonly used approximations. Part II. Estimating systematic biases in the best-fit parameters”, [Journal of Cosmology and Astroparticle Physics](#) **2020** no. 10, (Oct, 2020) 017–017.
- [92] N. Kaiser, “On the spatial correlations of Abell clusters”, [The Astrophysical Journal](#) **284** (1984) L9–L12.
- [93] J. M. Bardeen, J. Bond, N. Kaiser, and A. Szalay, “The statistics of peaks of Gaussian random fields”, [The Astrophysical Journal](#) **304** (1986) 15–61.
- [94] H. J. Mo and S. D. M. White, “An analytic model for the spatial clustering of dark matter haloes”, [Monthly Notices of the Royal Astronomical Society](#) **282** no. 2, (1996) 347–361, [arXiv:astro-ph/9512127](#).
- [95] S. Matarrese, P. Coles, F. Lucchin, and L. Moscardini, “Redshift evolution of clustering”, [Monthly Notices of the Royal Astronomical Society](#) **286** no. 1, (03, 1997) 115–132, [arXiv:astro-ph/9608004](#).
- [96] A. Dekel and O. Lahav, “Stochastic Nonlinear Galaxy Biasing”, [The Astrophysical Journal](#) **520** no. 1, (Jul, 1999) 24–34, [arXiv:astro-ph/9806193](#).
- [97] A. J. Benson, S. Cole, C. S. Frenk, C. M. Baugh, and C. G. Lacey, “The nature of galaxy bias and clustering”, [Monthly Notices of the Royal Astronomical Society](#) **311** no. 4, (02, 2000) 793–808, [arXiv:astro-ph/9903343](#).
- [98] J. A. Peacock and R. E. Smith, “Halo occupation numbers and galaxy bias”, [Monthly Notices of the Royal Astronomical Society](#) **318** no. 4, (11, 2000) 1144–1156, [arXiv:astro-ph/0005010](#).
- [99] V. Desjacques, D. Jeong, and F. Schmidt, “Large-scale galaxy bias”, [Physics Reports](#) **733** (2018) 1 – 193.
- [100] E. L. Turner, J. P. Ostriker, and J. R. Gott, III, “The statistics of gravitational lenses - The distributions of image angular separations and lens redshifts”, [Astrophysical Journal](#) **284** (Sep, 1984) 1–22.
- [101] A. Challinor and A. Lewis, “Linear power spectrum of observed source number counts”, [Phys. Rev. D](#) **84** (Aug, 2011) 043516, [arXiv:1105.5292](#).

- [102] D. Jeong, F. Schmidt, and C. M. Hirata, “Large-scale clustering of galaxies in general relativity”, [*Phys. Rev. D* **85** \(Jan, 2012\) 023504](#), [arXiv:1107.5427](#).
- [103] D. Bertacca, R. Maartens, A. Raccanelli, and C. Clarkson, “Beyond the plane-parallel and Newtonian approach: wide-angle redshift distortions and convergence in general relativity”, [*Journal of Cosmology and Astroparticle Physics* **2012** no. 10, \(2012\) 025](#), [arXiv:1205.5221](#).
- [104] D. Reitze, R. X. Adhikari, S. Ballmer, B. Barish, L. Barsotti, G. Billingsley, D. A. Brown, Y. Chen, D. Coyne, R. Eisenstein, et al., “Cosmic explorer: the US contribution to gravitational-wave astronomy beyond LIGO”, [arXiv preprint arXiv:1907.04833](#) (2019) .
- [105] L. Boco, A. Lapi, S. Goswami, F. Perrotta, C. Baccigalupi, and L. Danese, “Merging Rates of Compact Binaries in Galaxies: Perspectives for Gravitational Wave Detections”, [*The Astrophysical Journal* **881** no. 2, \(Aug., 2019\) 157](#), [arXiv:1907.06841](#) [[astro-ph.GA](#)].
- [106] M. Dominik, K. Belczynski, C. Fryer, D. E. Holz, E. Berti, T. Bulik, I. Mandel, and R. O’Shaughnessy, “Double Compact Objects. II. Cosmological Merger Rates”, [*The Astrophysical Journal* **779** no. 1, \(Dec., 2013\) 72](#), [arXiv:1308.1546](#) [[astro-ph.HE](#)].
- [107] M. Dominik, E. Berti, R. O’Shaughnessy, I. Mandel, K. Belczynski, C. Fryer, D. E. Holz, T. Bulik, and F. Pannarale, “Double Compact Objects III: Gravitational-wave Detection Rates”, [*The Astrophysical Journal* **806** no. 2, \(June, 2015\) 263](#), [arXiv:1405.7016](#) [[astro-ph.HE](#)].
- [108] S. E. de Mink, N. Langer, R. G. Izzard, H. Sana, and A. de Koter, “The Rotation Rates of Massive Stars: The Role of Binary Interaction through Tides, Mass Transfer, and Mergers”, [*The Astrophysical Journal* **764** no. 2, \(Feb., 2013\) 166](#), [arXiv:1211.3742](#) [[astro-ph.SR](#)].
- [109] M. Spera, M. Mapelli, and A. Bressan, “The mass spectrum of compact remnants from the PARSEC stellar evolution tracks”, [*Monthly Notices of the Royal Astronomical Society* **451** no. 4, \(Aug., 2015\) 4086–4103](#), [arXiv:1505.05201](#) [[astro-ph.SR](#)].
- [110] M. Spera and M. Mapelli, “Very massive stars, pair-instability supernovae and intermediate-mass black holes with the SEVN code”, [*Monthly Notices of the Royal Astronomical Society* **470** no. 4, \(Oct., 2017\) 4739–4749](#), [arXiv:1706.06109](#) [[astro-ph.SR](#)].
- [111] M. Spera, M. Mapelli, N. Giacobbo, A. A. Trani, A. Bressan, and G. Costa, “Merging black hole binaries with the SEVN code”, [*Monthly Notices of the Royal Astronomical Society* **485** no. 1, \(May, 2019\) 889–907](#), [arXiv:1809.04605](#) [[astro-ph.HE](#)].
- [112] N. Giacobbo and M. Mapelli, “The progenitors of compact-object binaries: impact of metallicity, common envelope and natal kicks”, [*Monthly Notices of the Royal Astronomical Society* **480** no. 2, \(Oct., 2018\) 2011–2030](#), [arXiv:1806.00001](#) [[astro-ph.HE](#)].
- [113] K. Belczynski, M. Dominik, T. Bulik, R. O’Shaughnessy, C. Fryer, and D. E. Holz, “The Effect of Metallicity on the Detection Prospects for Gravitational Waves”, [*The Astrophysical Journal Letters* **715** no. 2, \(2010\) L138](#), [arXiv:1004.0386](#).
- [114] A. Lamberts, S. Garrison-Kimmel, D. R. Clausen, and P. F. Hopkins, “When and where did GW150914 form?”, [*Monthly Notices of the Royal Astronomical Society* **463** no. 1, \(Nov., 2016\) L31–L35](#), [arXiv:1605.08783](#) [[astro-ph.HE](#)].
- [115] L. Cao, Y. Lu, and Y. Zhao, “Host galaxy properties of mergers of stellar binary black holes and their implications for advanced LIGO gravitational wave sources”, [*Monthly Notices of the Royal Astronomical Society* **474** no. 4, \(Mar., 2018\) 4997–5007](#), [arXiv:1711.09190](#) [[astro-ph.GA](#)].
- [116] O. D. Elbert, J. S. Bullock, and M. Kaplinghat, “Counting black holes: The cosmic stellar remnant population and implications for LIGO”, [*Monthly Notices of the Royal Astronomical Society* **473** no. 1, \(Jan., 2018\) 1186–1194](#), [arXiv:1703.02551](#) [[astro-ph.GA](#)].

- [117] S.-S. Li, S. Mao, Y. Zhao, and Y. Lu, “Gravitational lensing of gravitational waves: a statistical perspective”, [Monthly Notices of the Royal Astronomical Society](#) **476** no. 2, (May, 2018) 2220–2229, [arXiv:1802.05089](#) [astro-ph.CO].
- [118] C. J. Neijssel, A. Vigna-Gómez, S. Stevenson, J. W. Barrett, S. M. Gaebel, F. S. Broekgaarden, S. E. de Mink, D. Szécsi, S. Vinciguerra, and I. Mandel, “The effect of the metallicity-specific star formation history on double compact object mergers”, [Monthly Notices of the Royal Astronomical Society](#) **490** no. 3, (Dec., 2019) 3740–3759, [arXiv:1906.08136](#) [astro-ph.SR].
- [119] R. Abbott, T. Abbott, S. Abraham, F. Acernese, K. Ackley, A. Adams, C. Adams, R. Adhikari, V. Adya, C. Affeldt, et al., “Population Properties of Compact Objects from the Second LIGO-Virgo Gravitational-Wave Transient Catalog”, [arXiv preprint arXiv:2010.14533](#) (2020).
- [120] R. Aversa, A. Lapi, G. de Zotti, F. Shankar, and L. Danese, “Black Hole and Galaxy Coevolution from Continuity Equation and Abundance Matching”, [The Astrophysical Journal](#) **810** no. 1, (Sept., 2015) 74, [arXiv:1507.07318](#) [astro-ph.GA].
- [121] P. E. Dewdney, P. J. Hall, R. T. Schilizzi, and T. J. L. W. Lazio, “The Square Kilometre Array”, [Proceedings of the IEEE](#) **97** no. 8, (2009) 1482–1496.
- [122] A. Hall, C. Bonvin, and A. Challinor, “Testing general relativity with 21-cm intensity mapping”, [Phys. Rev. D](#) **87** (Mar, 2013) 064026.
- [123] N. H. M. Crighton, M. T. Murphy, J. X. Prochaska, G. Worseck, M. Rafelski, G. D. Becker, S. L. Ellison, M. Fumagalli, S. Lopez, A. Meiksin, and J. M. O’Meara, “The neutral hydrogen cosmological mass density at $z = 5$ ”, [Monthly Notices of the Royal Astronomical Society](#) **452** no. 1, (07, 2015) 217–234.
- [124] R. A. Battye, I. W. A. Browne, C. Dickinson, G. Heron, B. Maffei, and A. Pourtsidou, “HI intensity mapping: a single dish approach”, [Monthly Notices of the Royal Astronomical Society](#) **434** no. 2, (07, 2013) 1239–1256.
- [125] M. Spinelli, A. Zoldan, G. De Lucia, L. Xie, and M. Viel, “The atomic hydrogen content of the post-reionization Universe”, [Monthly Notices of the Royal Astronomical Society](#) **493** no. 4, (03, 2020) 5434–5455.
- [126] F. Villaescusa-Navarro, S. Genel, E. Castorina, A. Obuljen, D. N. Spergel, L. Hernquist, D. Nelson, I. P. Carucci, A. Pillepich, F. Marinacci, et al., “Ingredients for 21 cm intensity mapping”, [The Astrophysical Journal](#) **866** no. 2, (2018) 135.
- [127] A. M. Martin, E. Papastergis, R. Giovanelli, M. P. Haynes, C. M. Springob, and S. Stierwalt, “The Arecibo Legacy Fast ALFA Survey: X. The HI Mass Function and Ω_{HI} From the 40% ALFALFA Survey”, [The Astrophysical Journal](#) **723** no. 2, (Oct, 2010) 1359–1374. <https://doi.org/10.1088/0004-637x/723/2/1359>.
- [128] E. Castorina and F. Villaescusa-Navarro, “On the spatial distribution of neutral hydrogen in the Universe: bias and shot-noise of the HI power spectrum”, [Monthly Notices of the Royal Astronomical Society](#) **471** no. 2, (06, 2017) 1788–1796.
- [129] P. Bull, P. G. Ferreira, P. Patel, and M. G. Santos, “Late-time cosmology with 21 cm intensity mapping experiments”, [The Astrophysical Journal](#) **803** no. 1, (2015) 21.
- [130] E. R. Switzer, K. W. Masui, K. Bandura, et al., “Determination of $z \sim 0.8$ neutral hydrogen fluctuations using the 21 cm intensity mapping autocorrelation”, [Monthly Notices of the Royal Astronomical Society: Letters](#) **434** no. 1, (06, 2013) L46–L50.
- [131] L. Wolz, A. Pourtsidou, K. W. Masui, T.-C. Chang, J. E. Bautista, E.-M. Müller, S. Avila, D. Bacon, W. J. Percival, S. Cunnington, et al., “HI constraints from the cross-correlation of eBOSS galaxies and Green Bank Telescope intensity maps”, [arXiv preprint arXiv:2102.04946](#) (2021).

- [132] D. Alonso, P. Bull, P. G. Ferreira, and M. G. Santos, “Blind foreground subtraction for intensity mapping experiments”, [Monthly Notices of the Royal Astronomical Society](#) **447** no. 1, (12, 2014) 400–416.
- [133] I. P. Carucci, M. O. Irfan, and J. Bobin, “Recovery of 21 cm intensity maps with sparse component separation”, [Monthly Notices of the Royal Astronomical Society](#) (Sept., 2020) , [arXiv:2006.05996 \[astro-ph.CO\]](#).
- [134] S. Cunnington, M. O. Irfan, I. P. Carucci, A. Pourtsidou, and J. Bobin, “21-cm foregrounds and polarization leakage: cleaning and mitigation strategies”, [Monthly Notices of the Royal Astronomical Society](#) **504** no. 1, (June, 2021) 208–227, [arXiv:2010.02907 \[astro-ph.CO\]](#).
- [135] S. D. Matshawule, M. Spinelli, M. G. Santos, and S. Ngobese, “Hi intensity mapping with MeerKAT: Primary beam effects on foreground cleaning”, [arXiv e-prints](#) (Nov., 2020) [arXiv:2011.10815](#), [arXiv:2011.10815 \[astro-ph.CO\]](#).
- [136] P. S. Soares, C. A. Watkinson, S. Cunnington, and A. Pourtsidou, “Gaussian Process Regression for foreground removal in HI intensity mapping experiments”, [arXiv e-prints](#) (May, 2021) [arXiv:2105.12665](#), [arXiv:2105.12665 \[astro-ph.CO\]](#).
- [137] S. Camera, I. Harrison, A. Bonaldi, and M. L. Brown, “SKA weak lensing – III. Added value of multiwavelength synergies for the mitigation of systematics”, [Monthly Notices of the Royal Astronomical Society](#) **464** no. 4, (10, 2016) 4747–4760.
- [138] M. Spinelli, I. P. Carucci, S. Cunnington, S. E. Harper, M. O. Irfan, J. Fonseca, A. Pourtsidou, and L. Wolz, “SKAO HI Intensity Mapping: Blind Foreground Subtraction Challenge”, [arXiv e-prints](#) (July, 2021) [arXiv:2107.10814](#), [arXiv:2107.10814 \[astro-ph.CO\]](#).
- [139] B. F. Schutz, “Determining the Hubble constant from gravitational wave observations”, [Nature](#) **323** no. 6086, (1986) 310–311.
- [140] D. Bertacca, A. Raccanelli, N. Bartolo, and S. Matarrese, “Cosmological perturbation effects on gravitational-wave luminosity distance estimates”, [Physics of the Dark Universe](#) **20** (2018) 32–40.
- [141] S. Mukherjee, B. D. Wandelt, and J. Silk, “Testing the general theory of relativity using gravitational wave propagation from dark standard sirens”, [Monthly Notices of the Royal Astronomical Society](#) **502** no. 1, (01, 2021) 1136–1144.
- [142] Planck Collaboration, Ade, P. A. R., et al., “Planck 2015 results - XIII. Cosmological parameters”, [A&A](#) **594** (2016) A13, [arXiv:1502.01589](#).
- [143] K. K. Y. Ng, S. Vitale, W. M. Farr, and C. L. Rodriguez, “Probing Multiple Populations of Compact Binaries with Third-generation Gravitational-wave Detectors”, [The Astrophysical Journal Letters](#) **913** no. 1, (May, 2021) L5.
- [144] N. Aghanim, Y. Akrami, M. Ashdown, J. Aumont, C. Baccigalupi, M. Ballardini, A. Banday, R. Barreiro, N. Bartolo, S. Basak, et al., “Planck 2018 results-VI. Cosmological parameters”, [Astronomy & Astrophysics](#) **641** (2020) A6.
- [145] S. Alam et al., “The clustering of galaxies in the completed SDSS-III Baryon Oscillation Spectroscopic Survey: cosmological analysis of the DR12 galaxy sample”, [Monthly Notices of the Royal Astronomical Society](#) **470** no. 3, (03, 2017) 2617–2652.
- [146] G. F. Giudice, M. McCullough, and T. You, “Self-Organised Localisation”, [arXiv:2105.08617 \[hep-ph\]](#).
- [147] L. Heisenberg, M. Bartelmann, R. Brandenberger, and A. Refregier, “Dark energy in the swampland”, [Phys. Rev. D](#) **98** (Dec, 2018) 123502.
- [148] A. Raccanelli, “Gravitational wave astronomy with radio galaxy surveys”, [Monthly Notices of the Royal Astronomical Society](#) **469** no. 1, (04, 2017) 656–670.

- [149] A. Blanchard, S. Camera, C. Carbone, V. Cardone, S. Casas, S. Clesse, S. Ilić, M. Kilbinger, T. Kitching, M. Kunz, *et al.*, “Euclid preparation-VII. Forecast validation for Euclid cosmological probes”, [Astronomy & Astrophysics](#) **642** (2020) A191.
- [150] Ž. Ivezić *et al.*, “LSST: From Science Drivers to Reference Design and Anticipated Data Products”, [The Astrophysical Journal](#) **873** no. 2, (Mar, 2019) 111.
- [151] A. Bonaldi, I. Harrison, S. Camera, and M. L. Brown, “SKA weak lensing– II. Simulated performance and survey design considerations”, [Monthly Notices of the Royal Astronomical Society](#) **463** no. 4, (08, 2016) 3686–3698.
- [152] S. Hawking, “Gravitationally collapsed objects of very low mass”, [Monthly Notices of the Royal Astronomical Society](#) **152** no. 1, (1971) 75–78.
- [153] B. J. Carr and S. W. Hawking, “Black holes in the early Universe”, [Monthly Notices of the Royal Astronomical Society](#) **168** no. 2, (1974) 399–415.
- [154] A. Polnarev and R. Zembowicz, “Formation of primordial black holes by cosmic strings”, [Phys. Rev. D](#) **43** (Feb, 1991) 1106–1109.
- [155] S. Hawking, “Black holes from cosmic strings”, [Physics Letters B](#) **231** no. 3, (1989) 237 – 239.
- [156] U. F. Wichoski, J. H. MacGibbon, and R. H. Brandenberger, “Astrophysical constraints on primordial black hole formation from collapsing cosmic strings”, [Physics Reports](#) **307** no. 1, (1998) 191 – 196.
- [157] V. Berezin, V. Kuzmin, and I. Tkachev, “Thin-wall vacuum domain evolution”, [Physics Letters B](#) **120** no. 1, (1983) 91 – 96.
- [158] J. Ipser and P. Sikivie, “Gravitationally repulsive domain wall”, [Phys. Rev. D](#) **30** (Aug, 1984) 712–719.
- [159] P. Ivanov, P. Naselsky, and I. Novikov, “Inflation and primordial black holes as dark matter”, [Phys. Rev. D](#) **50** (Dec, 1994) 7173–7178.
- [160] J. García-Bellido, A. Linde, and D. Wands, “Density perturbations and black hole formation in hybrid inflation”, [Phys. Rev. D](#) **54** (Nov, 1996) 6040–6058, [arXiv:astro-ph/9605094](#).
- [161] P. Ivanov, “Nonlinear metric perturbations and production of primordial black holes”, [Phys. Rev. D](#) **57** (Jun, 1998) 7145–7154, [arXiv:astro-ph/9708224](#).
- [162] M. Crawford and D. N. Schramm, “Spontaneous generation of density perturbations in the early Universe”, [Nature](#) **298** (1982) 538–540.
- [163] D. La and P. J. Steinhardt, “Bubble percolation in extended inflationary models”, [Physics Letters B](#) **220** no. 3, (1989) 375 – 378.
- [164] I. Musco, J. C. Miller, and L. Rezzolla, “Computations of primordial black-hole formation”, [Classical and Quantum Gravity](#) **22** no. 7, (Mar, 2005) 1405–1424.
- [165] P. S. Cole and C. T. Byrnes, “Extreme scenarios: the tightest possible constraints on the power spectrum due to primordial black holes”, [Journal of Cosmology and Astroparticle Physics](#) **2018** no. 02, (Feb, 2018) 019–019.
- [166] A. Kalaja, N. Bellomo, N. Bartolo, D. Bertacca, S. Matarrese, I. Musco, A. Raccanelli, and L. Verde, “From primordial black holes abundance to primordial curvature power spectrum (and back)”, [Journal of Cosmology and Astroparticle Physics](#) **2019** no. 10, (Oct, 2019) 031–031.
- [167] I. Musco, “Threshold for primordial black holes: Dependence on the shape of the cosmological perturbations”, [Phys. Rev. D](#) **100** (Dec, 2019) 123524.
- [168] S. Young, I. Musco, and C. T. Byrnes, “Primordial black hole formation and abundance: contribution from the non-linear relation between the density and curvature perturbation”, [Journal of Cosmology and Astroparticle Physics](#) **2019** no. 11, (Nov, 2019) 012–012.

- [169] C. T. Byrnes, P. S. Cole, and S. P. Patil, “Steepest growth of the power spectrum and primordial black holes”, [Journal of Cosmology and Astroparticle Physics](#) **2019** no. 06, (Jun, 2019) 028–028.
- [170] G. Sato-Polito, E. D. Kovetz, and M. Kamionkowski, “Constraints on the primordial curvature power spectrum from primordial black holes”, [Phys. Rev. D](#) **100** (Sep, 2019) 063521. <https://link.aps.org/doi/10.1103/PhysRevD.100.063521>.
- [171] J. B. Muñoz, E. D. Kovetz, A. Raccanelli, M. Kamionkowski, and J. Silk, “Towards a measurement of the spectral runnings”, [Journal of Cosmology and Astroparticle Physics](#) **2017** no. 05, (May, 2017) 032–032.
- [172] H. Motohashi and W. Hu, “Primordial black holes and slow-roll violation”, [Phys. Rev. D](#) **96** (Sep, 2017) 063503.
- [173] A. D. Gow, C. T. Byrnes, and A. Hall, “Primordial black holes from narrow peaks and the skew-lognormal distribution”, [arXiv preprint arXiv:2009.03204](#) (2020) .
- [174] I. Musco, V. De Luca, G. Franciolini, and A. Riotto, “Threshold for primordial black holes. II. A simple analytic prescription”, [Phys. Rev. D](#) **103** (Mar, 2021) 063538.
- [175] C. T. Byrnes, E. J. Copeland, and A. M. Green, “Primordial black holes as a tool for constraining non-Gaussianity”, [Phys. Rev. D](#) **86** (Aug, 2012) 043512.
- [176] K. Inomata, E. McDonough, and W. Hu, “Primordial Black Holes Arise When The Inflaton Falls”, [arXiv preprint arXiv:2104.03972](#) (2021) .
- [177] S. Bird, I. Cholis, J. B. Muñoz, Y. Ali-Haïmoud, M. Kamionkowski, E. D. Kovetz, A. Raccanelli, and A. G. Riess, “Did LIGO Detect Dark Matter?”, [Phys. Rev. Lett.](#) **116** (May, 2016) 201301, [arXiv:1603.00464](#).
- [178] S. Clesse and J. García-Bellido, “The clustering of massive Primordial Black Holes as Dark Matter: Measuring their mass distribution with advanced LIGO”, [Physics of the Dark Universe](#) **15** no. Supplement C, (2017) 142 – 147, [arXiv:1603.05234](#).
- [179] T. D. Brandt, “Constraints on MACHO Dark Matter from Compact Stellar Systems in Ultra-faint Dwarf Galaxies”, [ApJ Letters](#) **824** no. 2, (2016) L31, [arXiv:1605.03665](#).
- [180] J. B. Muñoz, E. D. Kovetz, L. Dai, and M. Kamionkowski, “Lensing of Fast Radio Bursts as a Probe of Compact Dark Matter”, [Phys. Rev. Lett.](#) **117** (Aug, 2016) 091301.
- [181] A. M. Green, “Microlensing and dynamical constraints on primordial black hole dark matter with an extended mass function”, [Phys. Rev. D](#) **94** (Sep, 2016) 063530.
- [182] M. Zumalacarregui and U. Seljak, “Limits on stellar-mass compact objects as dark matter from gravitational lensing of type Ia supernovae”, [Phys. Rev. Lett.](#) **121** no. 14, (2018) 141101.
- [183] R. Murgia, G. Scelfo, M. Viel, and A. Raccanelli, “Lyman- α Forest Constraints on Primordial Black Holes as Dark Matter”, [Phys. Rev. Lett.](#) **123** (Aug, 2019) 071102.
- [184] Y. Ali-Haïmoud, E. D. Kovetz, and M. Kamionkowski, “Merger rate of primordial black-hole binaries”, [Phys. Rev. D](#) **96** (Dec, 2017) 123523.
- [185] V. De Luca, G. Franciolini, and A. Riotto, “NANOGrav Data Hints at Primordial Black Holes as Dark Matter”, [Phys. Rev. Lett.](#) **126** (Jan, 2021) 041303.
- [186] S. Mukherjee and J. Silk, “Can we distinguish astrophysical from primordial black holes via the stochastic gravitational wave background?”, [arXiv preprint arXiv:2105.11139](#) (2021) .
- [187] J. Adamek, C. T. Byrnes, M. Gosenca, and S. Hotchkiss, “WIMPs and stellar-mass primordial black holes are incompatible”, [Phys. Rev. D](#) **100** (Jul, 2019) 023506.
- [188] B. Carr, F. Kühnel, and M. Sandstad, “Primordial black holes as dark matter”, [Phys. Rev. D](#) **94** (Oct, 2016) 083504.

- [189] M. Sasaki, T. Suyama, T. Tanaka, and S. Yokoyama, “Primordial black holes—perspectives in gravitational wave astronomy”, [Classical and Quantum Gravity](#) **35** no. 6, (Feb, 2018) 063001, [arXiv:1801.05235](#).
- [190] A. M. Green and B. J. Kavanagh, “Primordial black holes as a dark matter candidate”, [Journal of Physics G: Nuclear and Particle Physics](#) **48** no. 4, (Feb, 2021) 043001.
- [191] B. Carr and J. Silk, “Primordial black holes as generators of cosmic structures”, [MNRAS](#) **478** no. 3, (05, 2018) 3756–3775, [arXiv:1801.00672](#).
- [192] B. Carr and F. Kühnel, “Primordial Black Holes as Dark Matter: Recent Developments”, [Annual Review of Nuclear and Particle Science](#) **70** no. 1, (2020) 355–394.
- [193] M. Raidal, C. Spethmann, V. Vaskonen, and H. Veermäe, “Formation and evolution of primordial black hole binaries in the early universe”, [Journal of Cosmology and Astroparticle Physics](#) **2019** no. 02, (Feb, 2019) 018–018.